Deep-Sea Research, Vol. 35, No. 9, pp. 1451–1482, 1988.
Printed in Great Britain.

0198–0149/88 $3.00 + 0.00

On the circulation of the upper waters in the western equatorial Pacific Ocean

J. M. TOOLE,* E. ZOU† and R. C. MILLARD*

(*Received* 10 *September* 1987; *in revised form* 25 *February* 1988; *accepted* 5 *April* 1988)

Abstract—Historical hydrographic data and CTD/O_2 observations obtained on two recent cruises are used to investigate the circulation of the upper waters of the western equatorial Pacific Ocean. The study area lies between 20°N and the land boundary of the Papua New Guinea–Solomon Island coasts, 170°E and the Philippine coast. Seasonal mean and annual averaged sections are constructed from the historical data set to address the strength of the major equatorial currents and the water mass budget of the far western region of the study area. We find indication of significant contribution of southern hemisphere waters to the North Equatorial Countercurrent with an inferred Pacific to Indian Ocean throughflow of Mindanao Current waters of order 1 Sv. The recent observations, acquired under the auspices of a cooperative program between the United States and People's Republic of China, were collected in January–February and November–December 1986. The thermohaline structure of the various currents and net transports estimated for the 1986 data sets are examined and compared with the historical mean data. Large differences are seen between the two modern sections obtained along 165°E. These reflect high frequency variability (as demonstrated by comparison with a third section obtained 2 weeks prior to the January–February cruise) and interannual variability (the second of the cruises occurred during the onset of the 1986–1987 El Niño event).

1. INTRODUCTION

THE western equatorial Pacific Ocean is characterized by a vigorous and complex near-surface circulation. The North Equatorial Current (NEC), upon reaching the western boundary, bifurcates; the northern branch feeds the Kuroshio Current, while the southern limb constitutes the Mindanao Current (see NITANI, 1972). The bulk of the Mindanao Current is in turn thought to deflect to the east off the southern Philippine coast and supply the North Equatorial Countercurrent (NECC) (WYRTKI, 1961). Based on water mass properties, WYRTKI (1961), GORDON (1986) and FINE (1985) argue that a portion of the Mindanao Current turns west to supply the Indonesian throughflow. The NECC in the western Pacific, located between the equator and 10°N, varies seasonally in response to wind forcing. Largest NECC transport is believed to occur in boreal autumn and weakest transport in spring (e.g. WYRTKI, 1961). The surface flow south of the equator is also thought to vary seasonally: directed to the east along the Papua New Guinea coast in boreal winter and to the west in other seasons (WYRTKI, 1961). Recently, the Western Equatorial Pacific Ocean Circulation Study (WEPOCS) discovered a westward directed subsurface flow along the Papua New Guinea coast, independent from the surface flow (LINDSTROM *et al.*, 1987). This subsurface current, which transports highly saline water, is

* Department of Physical Oceanography, Woods Hole Oceanographic Institution, Woods Hole, MA 02543, U.S.A.
† 1st Institute of Oceanography, State Oceanic Administration, Qingdao, People's Republic of China.

believed to feed the Equatorial Undercurrent (EUC). Relatively little is known about the EUC and the zonal pressure gradient in this area. Direct velocity observations have documented eastward directed flow in the thermocline at the equator east of 150°E (LINDSTROM *et al.*, 1987; DELCROIX *et al.*, 1987; M. MCPHADEN, personal communication). A companion study of the zonal pressure gradient in the area is now underway (L. MANGUM, personal communication).

Presently, a series of oceanographic cruises are being staged in the western Pacific to better document these currents and to characterize their seasonal and interannual variability. As background to the modern data, a study of the existing hydrographic data from the area was undertaken. Seasonal and annual mean sections were constructed and transports of the major surface currents estimated. As such, the analysis differs from those of KENDALL (1969) and NITANI (1972), who discussed sets of synoptic sections. The results of the present analysis are discussed in Section 2 below. Subsequently, the structures and transports observed on two synoptic cruises are examined (Section 3). The cruises, which occurred in January–February and November–December 1986, were part of the United States–People's Republic of China cooperative program in the western Pacific. The Appendix documents the treatment of the historical and modern observations and the methods of analysis.

2. HISTORICAL DATA ANALYSIS

Annual mean

Thermohaline stratification. Three annual mean meridional sections with 2° spatial resolution were constructed from the historical hydrographic data (see Appendix). Section A encompassed observations between 128° and 138°E, section B spanned 138–153°E, and section C covered 153–170°E (Fig. 1). The thermohaline structure of the three mean sections are quite similar in appearance; the easternmost section (area C) is presented in Fig. 2. The water mass characteristics of the western Pacific have been discussed extensively by REID (1965), TSUCHIYA (1968), NITANI (1972), MASUZAWA (1972), WANG *et al.* (1983), DELCROIX *et al.* (1987) and others. A few of the major features are noted here with reference to Fig. 2. The temperature distribution exhibits the well-developed shallow thermocline characteristic of the tropics, with latitudinal depth variations associated with the baroclinic equatorial current field. Mean surface temperatures are above 28°C south of roughly 10°N; the hydrographic data do not provide sufficient vertical resolution to quantify accurately the depth of the surface mixed layer. The ridge in the thermocline between the NEC and NECC is at 8°N in all three sections. A pronounced swelling of the thermocline is evident at the equator, indicative of the geostrophic signature of the eastward directed EUC. (This feature is not well developed on sections A and B.) South of the equator, the strength of the thermocline weakens with shallow isotherms sloping up to the south poleward of 4°S. Below the thermocline, lateral temperature gradients associated with the North and South Subsurface Countercurrents (NSSCC, SSSCC) are found around ±2° latitude, at about 400 db. The temperature field below 600 db is relatively flat equatorward of 10° latitude. Near 10°N however, deep isotherms appear to rise to the north although shallower isotherms are descending within the NEC.

The salinity field of the western Pacific has an extreme range. Low surface water salinities are found at 5–10°N, perhaps associated with the Intertropical Convergence

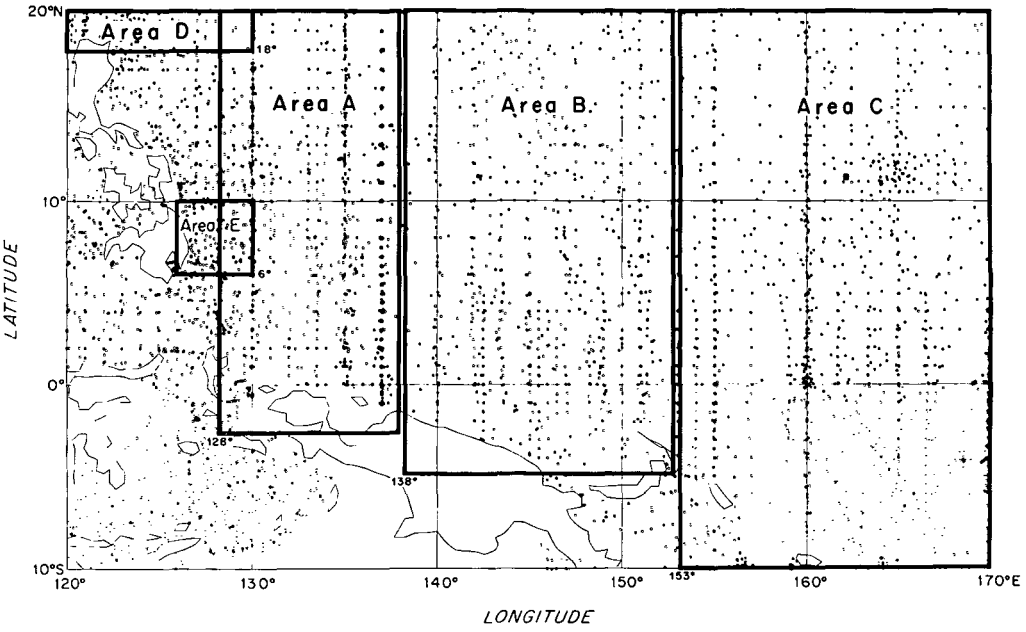

Fig. 1. Geographic distribution of all hydrographic stations used in the analysis of the mean circulation of the western equatorial Pacific Ocean. Average sections were constructed in five areas, labeled A–E. Seasonal and annual mean meridional sections were obtained for areas A, B and C; annual mean zonal sections were estimated from the data in areas D and E.

Zone (ITCZ); values fall below 34.3‰ in areas B and C and below 34.1‰ in area A. Eastward advection of Indonesian surface waters by the NECC also could be responsible for this feature (see below). The two subtropical water high salinity cores are seen between 150 and 200 db around a potential density value of 25 kg m^{-3}. Maximum salinity of the northern tongue exceeds 35.1‰ in areas B and C, and reaches nearly 35.0‰ in area A. The southern salinity maximum core achieves values above 35.7 in area C, 35.5 in B and 35.2 in A. (Extrema properties of thin features like the salinity maxima are subject to underestimation with hydrographic data because of their inherently poor vertical resolution.) A local salinity minimum at these density horizons is found between the two salinity maximum tongues, at the approximate location of the thermocline ridge between the NEC and NECC. The 35.0‰ isohaline extends south from the northern core in areas B and C to about 13°N and reaches north from the southern core to 4°N. Somewhat deeper at these latitudes a local salinity minimum in depth is seen, with values below 34.6‰ (TSUCHIYA, 1982). Below 500 db low salinity cores associated with North Pacific Intermediate Water (NPIW) to the north and Antarctic Intermediate Water (AAIW) to the south are found (REID, 1965). Salinity in the NPIW at 20°N falls below 34.2‰, increasing to somewhat above 34.5‰ at 10°N, comparable to the salinities found in the AAIW core. Dissolved oxygen and other water mass properties have been used to differentiate these waters of comparable salinity, see Section 3 below.

Annual mean zonal sections with 1° spatial resolution were also constructed from data at the western boundary, areas D and E in Fig. 1 (see Appendix). Previous studies have documented the bifurcation of the NEC at the Philippine coast with the northward

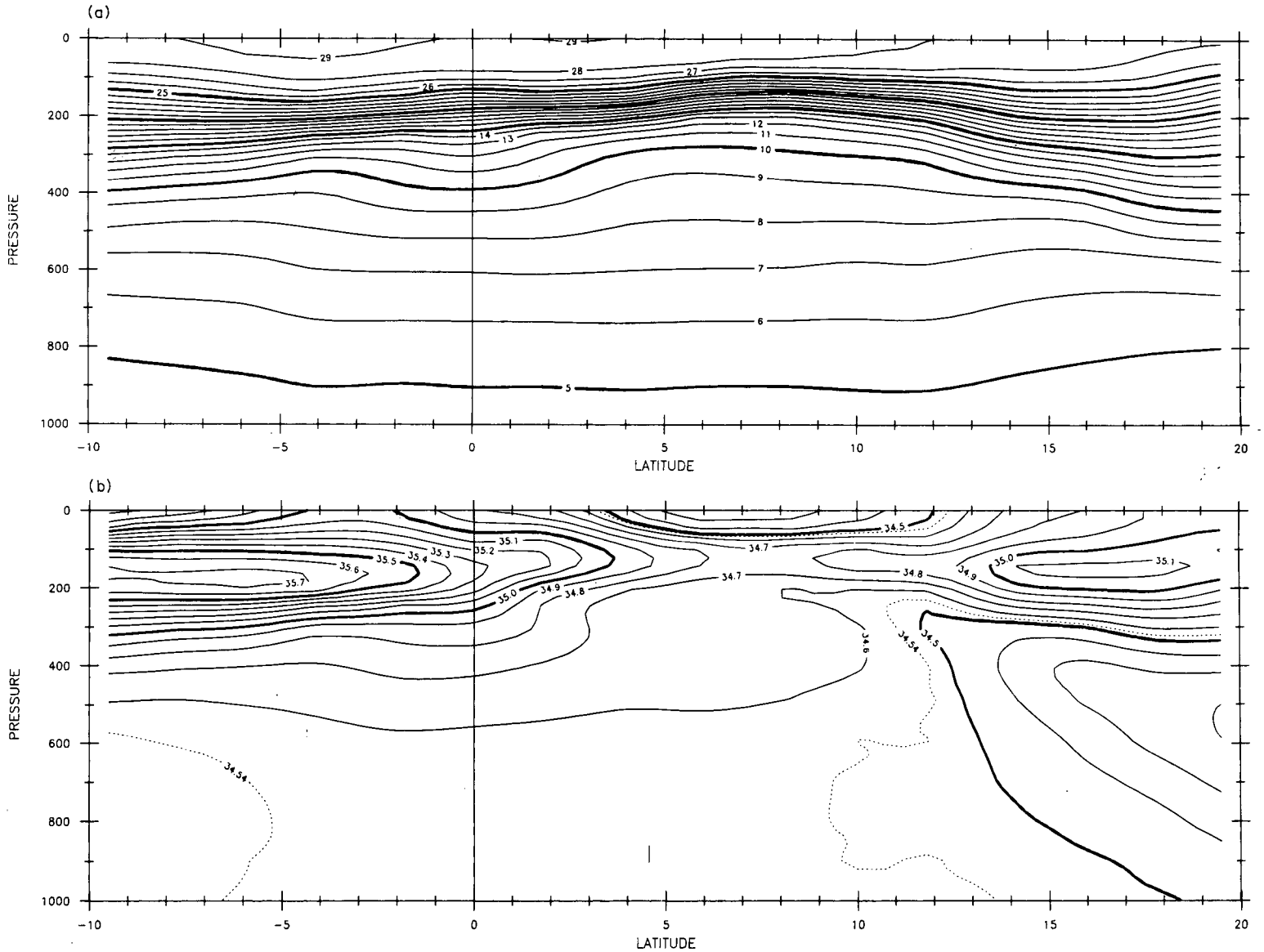
(a)
PRESSURE
0
200
400
600
800
1000
−10
−5
0
5
10
15
20
LATITUDE
29
28
27
26
25
14
13
12
11
10
9
8
7
6
5
(b)
PRESSURE
LATITUDE
35.7
35.6
35.5
35.4
35.3
35.2
35.1
35.0
34.9
34.8
34.7
34.6
34.5

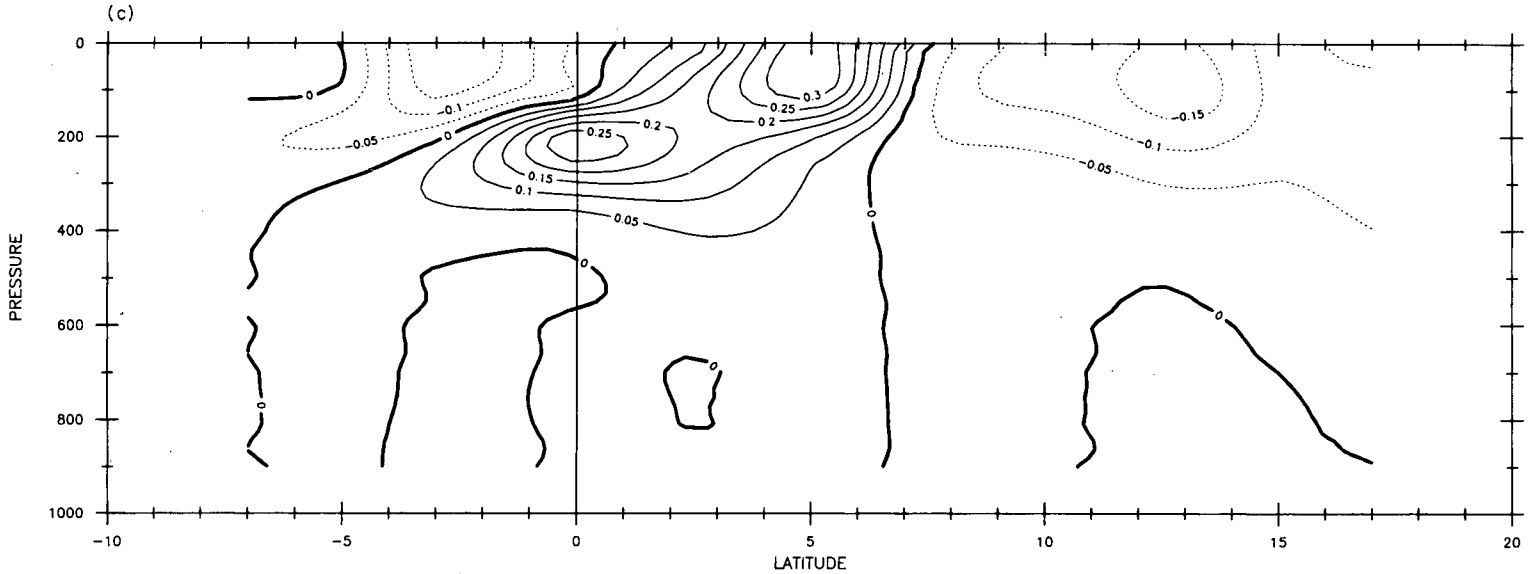

Fig. 2. Annual mean meridional sections of (a) temperature in °C and (b) salinity in ‰ for study area C (153°–170°E). The zonal geostrophic velocity (m s^{-1}) relative to 1000 db calculated from the data in (a) and (b) appears in (c). Solid contours denote eastward relative flow.

branch forming the Kuroshio Current and the southward branch constituting the Mindanao Current (NITANI, 1972). We therefore expected to find the thermocline sloping up sharply to the west on section D, reflecting the baroclinic structure of the Kuroshio. While the thermocline does slope up on the section, the gradients are not large and are confined near the coast. Conversely, the Mindanao appears much broader, the thermocline slopes down to the west rather uniformly west of 130°E.

The salinity fields observed on sections D and E closely resemble that of area A poleward of 8°N (not surprising given that the NEC is supplying the water observed at these sections). Within the Kuroshio, the lowest values of salinity at the subtropical water high salinity core are found at the coastal station (value approximately 34.8‰). Conversely, at the depths of the NPIW, highest salinity values are found at the coast (about 34.4‰). These zonal trends are reversed on the Mindanao Current section; highest salinity in the subtropical water and lowest NPIW salinities are at the coast with values approximately equal to those cited above. These distributions are consistent with a NEC bifurcation at a latitude around 12°N, as also discussed by NITANI (1972).

Velocity fields and circulation. The geostrophic velocity fields with respect to 1000 db on the annual mean sections strongly reflect the depth variations of the thermocline. Observations of the near-equatorial velocity field in the western Pacific were discussed by MAGNIER *et al.* (1973), HISARD *et al.* (1970) and more recently DELCROIX *et al.* (1987); here again major features are noted as review. The broad westward directed NEC is located poleward of 8°N (Fig. 2), achieving speeds of order 20 cm s^{-1} about 10–15°N. Below 500 db, weak eastward relative flow is indicated which is related to the opposing meridional isotherm slopes noted above. Eastward directed surface flow in the NECC is seen from 8°N to near the equator; its southern boundary is not particularly well resolved. [Velocity data are available at 3°N (gradient calculation between 2° and 4°N) and at the equator (from a dynamic height curvature estimator based on data between 2°N and 2°S).] Surface speeds in the NECC exceed 30 cm s^{-1} in area C, 35 cm s^{-1} in B and 50 cm s^{-1} in A. In each case the velocity extremum is found at about 5°N. Westward directed surface flow (South Equatorial Current, SEC) is calculated between the equator and 5°S on section C and a weak indication of the eastward South Equatorial Countercurrent (SECC) is seen farther south. Subsurface eastward flow is evident about 200 db near the equator, the EUC appears merged with the two SSCC's and the surface NECC. Discrimination between these flows is hampered by the resolution of the data. Finally, there is a tendency for weak westward flow at the equator below 400 db, perhaps indicative of the Equatorial Intermediate Current (EIC) thought to be well developed at these longitudes (MAGNIER *et al.*, 1973; DELCROIX and HENIN, 1988).

The baroclinic velocity field on section D is weak in general, away from the coast. Consistent northward flow is indicated only within 120 nmi of the Philippines, where a surface intensified current with speeds of 45 cm s^{-1} is observed. Relatively strong southward surface flow is found everywhere west of 130°E on section E with speeds exceeding 40 cm s^{-1}.

A circulation diagram for the annual mean flow in the western Pacific was constructed by estimating the major equatorial current transports of waters warmer than 12°C (see Appendix). The choice of the 12°C isotherm as a lower limit for the depth integration was motivated by the structure of the thermocline in the area: 12°C lies at the base of the strong vertical temperature gradient of the upper ocean. Consequently, vertical integration down to this surface captures the bulk of the surface current transport. In

addition, since the velocities are small at the depths occupied by the 12°C isotherm, weak cross-isotherm flow might be expected. Neither statement is valid for shallower surfaces.

The present results may be contrasted with the circulation diagrams given by KENDALL (1969) of transport between the surface and 500 db, NITANI (1972) of total transport relative to 1200 db, and the recent observations along 165°E discussed by DELCROIX *et al.* (1987), who estimated transport above the 23.5 kg m^{-3} sigma-*t* surface (23.5 kg m^{-3} roughly corresponds to the 25°C isotherm along 165°E).

The NEC in the present study appears to increase in transport to the west from 30 Sv at area C to 43 Sv at area A (Table 1). (NEC was defined as the westward current between 8° and 18°N, the northern limit of the present study.) MASUZAWA (1964) discussed how the transport increase to the west was consistent with the observed wind forcing and SVERDRUP (1947) dynamics. The annual mean net Sverdrup transport between 19° and 9°N based on the HELLERMAN and ROSENSTEIN (1983) wind stress data increases from 41 Sv in area C to 54 Sv in area A. Within the NEC the transport weighted mean temperature (see Appendix) is relatively constant (Table 1); the transport weighted salinity is smaller at section A than at B and C, in part because lower surface water salinity is found at section A.

The velocity fields on the three meridional sections were integrated between 8° and 2°N to establish NECC transports. (As noted earlier, the boundary betwen the NEC and NECC occurred at 8°N in the three sections and eastward flow extended south on all sections to at least 2°N. The southern limit of integration of 2°N was dictated by station resolution and stability of the geostrophic calculations.) The resulting volume transports are sizable, of order 30 Sv, decreasing downstream from area A to C (Table 1). Annual mean Sverdrup transport integrated between 1° and 9°N decreases from 36 Sv at section

Table 1. *Annual mean transport estimates for waters warmer than* 12°C *along with the transport weighted mean temperature and salinity values. Velocities were calculated relative to* 1000 db *and integrated over the given latitude ranges between the surface and the* 12°C *isotherm depth. Temperature and salinity transports were obtained by similar integration of the product of the velocity and the* T *and* S *fields. Transport weighted mean* T *and* S *are given by the ratio of the property transport to the volume transport. The equatorial transports are given for completeness but confidence in the geostrophically computed surface flow near the equator is low; the distinctly different transport weighted mean property values of the equatorial zone reflect flow reversals within the area of integration*

	Area A	Area B	Area C
NEC (8–18°N)	–42.6 Sv	–35.8 Sv	–30.4 Sv
	22.49°C	22.32°C	22.57°C
	34.61‰	34.77‰	34.77‰
NECC (2–8°N)	33.3 Sv	30.4 SV	24.3 Sv
	23.02°C	24.25°C	24.69°C
	34.73‰	34.78‰	34.75‰
Equator (2°S–2°N)	1.0 Sv	0.7 Sv	1.3 Sv
	11.82°C	11.43°C	16.75°C
	34.85‰	34.82‰	48.83‰
SEC (2–4,8°S)	–	–8.3 Sv	–8.1 Sv
B area to 4°S	–	25.59°C	26.05°C
C area to 8°S	–	35.14‰	35.38‰
Kuroshio (Area D)	15.3 Sv	20.75°C	34.62‰
Mindanao (Area E)	–17.5 Sv	22.08°C	34.54‰

A to 30 Sv at C. DELCROIX *et al.* (1987) report an average NECC transport based on six recent sections at 165°E of 27.4 Sv (where NECC is defined as all eastward flow north of 2°S above the 23.5 kg m^{-3} isopycnal). The present estimates of transport weighted mean temperature increase to the east, while the mean salinity is relatively constant.

Equatorial transports (integrations from 2°N to 2°S) were evaluated but are not given much credence as the ageostrophic wind-driven motion is not included. DELCROIX *et al.* (1987) discuss this using directly measured upper ocean velocity data. The net geostrophic transports are eastward in all three sections (Table 1). Flow reversals occur in this latitude band, so consequently the transport weighted mean temperature and salinity values differ strongly from those of the other currents. SEC transport was estimated as the net flow south of 2°S on sections B and C. Net westward transport is indicated on both sections. As noted in the Appendix, transport underestimation is suspected here as the mean sections do not resolve flow near the boundaries. (For example, the westward directed subsurface flow along the Papua New Guinea coast does not appear in the historical data.) The data of DELCROIX *et al.* (1987) give a net westward transport of 44 Sv when the velocity field (excluding the EUC) is integrated poleward to 16°S.

Net northward transport through section D across the Kuroshio is relatively small, only 15 Sv. NITANI (1972) reported a value of 30 Sv (surface to 1200 db) but Kendall obtained a value of only 19 Sv (surface to 500 db). A net southward directed transport of 17.5 Sv is computed through section E, transport weighted properties are given in Table 1. WYRTKI (1961) suggested the mean Mindanao Current carries 10 Sv (based on a subjective estimate of current width and vertical extent). NITANI (1972) reported Mindanao transport of 25 Sv with a recirculation about the Mindanao eddy and a depression of surface dynamic height around 130°E, of order 15 Sv (again 0–1200 db integration).

Given these transport data, the mass budget of the western Pacific surface water was examined. The study focused on the regions bounded by the Philippine coastal sections and section A (Fig. 3), similar to that studied by KENDALL (1969). Of the various current transport estimates, those of the NEC and NECC are felt most reliable as section A does an adequate job of resolving these flows. The raw data indicate a mass imbalance for the region between sections D and E; 43 Sv of NEC water enter the area and only 15 Sv of Kuroshio and 17 Sv of Mindanao water leave. To achieve mass balance, we apportion the residual of 11 Sv to the two coastal flows based on a NEC bifurcation latitude of 12°N as suggested by the water mass properties discussed above. (Kuroshio transport equals NEC transport north of 12°N, Mindanao transport equals that south.) The result shown schematically in Fig. 3 is a Mindanao Current transport of 18 Sv and a Kuroshio transport of 25 Sv. Consistent with a salt budget for the area, we accept the transport weighted mean temperature and salinity values for the coastal flows obtained from the raw data.

The mass budget for the area south of section E and west of section A is more complex. Entering the region are the Mindanao Current, and possibly flow south of 2°N across section A where the geostrophic calculations are unreliable. (Flow across section A south of 2°N is referred to as the SEC in the following.) Exiting are the NECC at section A and Indonesian throughflow between the Pacific and Indian oceans. Additionally the region is thought to experience a net gain of fresh water from precipitation and runoff exceeding evaporation (e.g. BAUMGARTNER and REICHEL, 1975). Of these, the magnitude of the time mean SEC flow is not known; estimates of the throughflow range from a few Sverdrups to nearly 20 Sv (GORDON, 1986). The fresh water input is also

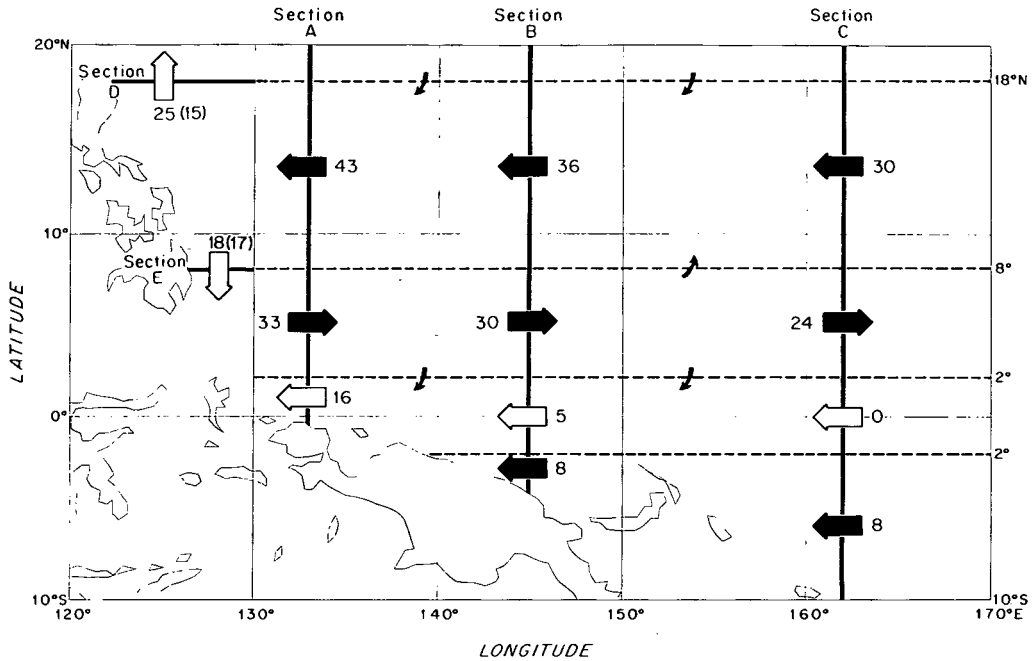

Fig. 3. A circulation diagram for the waters warmer than 12°C deduced from annual mean hydrographic sections and water mass budgets (transports in Sv). Bold typeface arrows represent directly calculated transports as discussed in the text. Open-faced arrows are transport values inferred from water mass budgets. Shown in parentheses are the transports computed directly for these sections with the available data.

highly uncertain. Mass and salt conservation constraints were applied to the region to try and infer the SEC and throughflow transports in terms of other (somewhat better) known transports.

The statement of mass conservation for the region takes the form:

$$M_{\text{mind}} + M_{\text{sec}} - M_{\text{necc}} - M_{\text{thru}} + F = 0, \tag{1}$$

where M_{mind}, M_{sec}, M_{necc} and M_{thru} are the mass transports of the Mindanao, SEC, NECC and throughflow, respectively, and F is the net fresh water input. No net flow across the 12°C isotherm is allowed in this model.

The salt budget constraints may be approximated by

$$M_{\text{mind}}S_{\text{mind}} + M_{\text{sec}}S_{\text{sec}} - M_{\text{necc}}S_{\text{necc}} - M_{\text{thru}}S_{\text{thru}} = 0, \tag{2}$$

where the S terms are the transport weighted mean salinities of the respective flows. From Table 1 we take the observed S_{necc} at section A and the value of $S_{\text{mind}} \cdot S_{\text{sec}}$ is taken from section B, with the expectation that the unresolved coastal flow may make this an underestimate. Sensitivity studies will be discussed below. From PIOLA and GORDON (1984) we take S_{thru} as 33.5‰ and for F the value of 0.1 Sv. Equations (1) and (2) yield

the following:

$$M_{sec} = \frac{S_{thru}(M_{mind} + F - M_{necc}) - S_{mind}M_{mind} + S_{necc}M_{necc}}{(S_{sec} - S_{thru})}$$

$$= \frac{33.5 \times (18\text{ Sv} + 0.1\text{ Sv} - 33\text{ Sv}) - 34.5 \times 18\text{ Sv} - 34.7 \times 33\text{ Sv}}{(35.1 - 33.5)}$$

$$= 15.6\text{ Sv}. \tag{3}$$

$$M_{thru} = M_{mind} + M_{sec} - M_{necc} + F$$

$$= 18 + 15.6 - 33 + 0.1 = 0.7\text{ Sv}. \tag{4}$$

Mass and salt conservation in the far western region of the Pacific requires a significant contribution of SEC waters to the NECC, a finding in fact suggested by KENDALL'S (1969) Fig. 4 and NITANI'S (1972) Fig. 28. Basically, this requirement stems from the large salinity transport of the NECC out of the area which, in turn, is a consequence of the high values of salinity in the southern part of this current. As no waters with this salinity are found in the Mindanao Current, the only remaining source is the southern hemisphere.

Sensitivity studies were performed to assess the uncertainties of these results in terms of the specified mass and salinity transport values. Specified volume transports were altered by 30% and transport weighted salinities by 0.5‰, values consistent with uncertainties in the estimated mean properties (see Appendix). The conclusion that SEC waters contribute significantly to the NECC is relatively robust; model solution values of M_{sec} were typically greater than 25% of M_{necc} for reasonable parameter choices. The magnitude of the throughflow transport estimate is rather sensitive (percentage wise) to the specified parameters. Larger values were obtained when NECC volume and salt transports were decreased. However, drastic changes are required to force a throughflow much larger than 5 Sv. These findings indicate that a throughflow of order 10 Sv as required by the large-scale water mass budget of PIOLA and GORDON (1984) cannot be supported in the present circulation scheme.

It is also relevant to examine what the circulation scheme discussed above implies for the heat budget of the area. The net heat gain in the region caused by ocean currents, Q, expressed here in terms of temperature transport divergence, is given by

$$Q = M_{mind}T_{mind} + M_{sec}T_{sec} - M_{necc}T_{necc} - M_{thru}T_{thru}, \tag{5}$$

where the T's are the respective transport weighted mean temperatures. Taking data from Table 1 with $T_{thru} = 26$°C we obtain

$$Q = 18\text{ Sv} \times 22.1\text{°C} + 15.6\text{ Sv} \times 25.6 - 33\text{ Sv} \times 23.0 - 0.7\text{ Sv} \times 26\text{°C}$$

$$= +18.9\text{°C Sv} = 8 \times 10^{13}\text{ W}.$$

The calculation indicates that ocean currents import heat to the study area which implies for steady state, the ocean must lose heat to the atmosphere on average. We note that the sign of this result is opposite that obtained from bulk aerodynamic formulae (e.g. WEARE *et al.*, 1981). Sensitivity studies were performed again to determine the confidence bounds to the present heat budget. Because the transport weighted mean temperature of the various currents supplying and removing mass from the study area are so similar, the

net heat budget represents a small difference between several large numbers, each of which is uncertain. By reducing T_{sec} by only 1.5°C or increasing the throughflow to order 5 Sv, the heat budget estimate changes sign. We conclude that the present analysis cannot establish the sign of the heat budget of the area.

Seasonal variations

The four seasonal mean sections from areas A, B and C were used to examine the seasonal cycle of the near-equatorial flows. Transports of the major currents (temperature >12°C) were estimated from dynamic height data computed from the seasonal mean temperature and salinity profiles (Table 2). Some care must be exercised in the interpretation of these results as the data distributions are uneven throughout the year. The data in Table 2 suggest little seasonal cycle in transport of the NEC, a finding consistent with NITANI (1972) and WYRTKI (1961). The range in transport between seasons averages 20% of the annual mean NEC transport, no consistent pattern is seen between when the minimum and maximum transport occurs on the three sections. The increase of NEC transport to the west does appear as a robust feature of the analysis as each season's data exhibit it. Data from areas B and C document a seasonal NECC transport cycle with minimum transport in March–May, and maximum transport in September–November, also consistent with previous investigations. The range in transport is 47% of the mean in area B and 118% in area C. Excluding the boreal autumn season data, the decrease of NECC transport to the east found in the annual mean sections is reproduced in the seasonal mean sections. The large, relatively steady NECC transport at area A may reflect steadiness of the Mindanao eddy. Strong recirculation about this feature could mask the seasonal wind-driven variability.

Poor spatial resolution and data coverage make difficult a study of flow seasonality along the Papua New Guinea coast. Historically a seasonally reversing surface flow has been described with eastward directed flow in boreal winter. Part of the observed surface current may be ageostrophic flow driven by the northwest monsoon. Geostrophic transport between 2° and 4°S at area B, while consistently westward throughout the year, achieves a minimum in March–May (–1.4 Sv as compared to the annual mean value of –8 Sv). The November–December–January 4°S average station exhibits unusually large surface dynamic height relative to deep surfaces, leading to a strong westward transport in this season. The representativeness of this mean station (formed from only 11 casts) to the true winter season mean is suspect.

Table 2. Seasonal mean zonal transport estimates (Sv) *for the NEC and NECC waters warmer than* 12°C. *Geostrophic velocity fields, estimated from dynamic height data relative to* 1000 db *were integrated in latitude between* 18°N *and the NEC/NECC boundary (for NEC transport) and between the NEC/NECC boundary and the first occurrence of surface westward flow or* 2°N *(for NECC transport)*

Season	NEC Area A	NEC Area B	NEC Area C	NECC Area A	NECC Area B	NECC Area C
D–J–F	–38.8	–34.0	–27.2	36.4	31.2	22.3
M–A–M	–45.9	–40.1	–30.6	32.3	23.3	13.2
J–J–A	–43.5	–43.1	–29.2	38.6	34.2	24.9
S–O–N	–43.4	–32.6	–25.8*	28.6	36.6	41.8

* Meridional integration between 8° and 14°N (insufficient data north of 15°N).

3. THE 1986 CRUISE RESULTS

Cruise 1: *January–February* 1986

165°E *Section*. Contoured sections of temperature, salinity, dissolved oxygen and zonal geostrophic velocity constructed from data obtained on the first cruise of the US/PRC program appear in Fig. 4. In general, these fields contain more structure than the historical data sections as finer station spacing was available (typically 1° resolution, narrowing to 1/2° within 3° of the equator, Fig. A1). Surface temperature exceeds 29°C on 165°E to the south of 5°N. Surface salinity is low at the northern end of the section (near 34.0), achieves maximum values of around 34.9 at 2°N and falls to below 34.5 at 6°S.

As was the case for the annual mean and November–December–January season structure discussed above, the thermocline ridge between the NEC and NECC is found at 8°N. However, the trough in the thermocline marking the southern boundary of the NECC is located at 4°N, poleward of its mean position. South of the equator, a local trough in thermocline depth is found around 5°S. Just south of the equator, a spreading of the thermocline is evident, the only indication in the CTD data of the EUC. On a larger scale, the thermocline tends to be bowed up about the equator indicating westward relative geostrophic flow, see below. The thermal gradients associated with the SSCC's are well resolved on the section with isotherms equatorward of these features bowed up at the equator.

The salinity field observed on 165°E is very similar to the area C annual mean section of Fig. 2, even in terms of extrema values. The southern hemisphere salinity maximum achieves values of 35.7 at the southern end of the section and appears to extend northward across the equator where the 35.0 isohaline reaches 5°N (vs 4°N in the annual mean section). The lower half of this core (potential density values between 25.0 and 26.5 kg m^{-3}) does not extend into the northern hemisphere but ends abruptly at a salinity front at the equator. The cruise did not extend far enough north to sample northern core salinity maximum values above 35.0. The shallow salinity minimum layer is well sampled, however, positioned at 200 db to the north of the equator. Lowest values, below 34.5, are found at the northern end of the section. The deep salinity minimum cores exhibit a weak latitudinal variation along the section with a local maximum between 4° and 6°N.

The dissolved oxygen field shows a significant meridional gradient at these depths. The AAIW to the south has dissolved oxygen values nearly 1 ml l^{-1} greater than those to the north (REID, 1965). A local oxygen maximum is found about 500 db at 6°S, where values are greater than 3 ml l^{-1}, suggestive of northward flow of relatively young AAIW along the Solomon Island arc. On the equator at these depths a local oxygen minimum is seen, most probably associated with the EIC (DELCROIX and HENIN, 1988). The SSCC's are associated with relatively high oxygen content as is the case to the east (TSUCHIYA, 1975; HAYES *et al.*, 1983). The southern salinity maximum is related to a local minimum in the oxygen vertical profile, with the low oxygen core lying somewhat deeper than the salinity core in the southern part of the section. Relatively low oxygen also is found below the thermocline about the boundary between the NEC and NECC.

The zonal velocity field with respect to 1000 db observed on cruise 1 is quite different from the historical mean sections. The NECC is bounded between 8° and 4°N, while

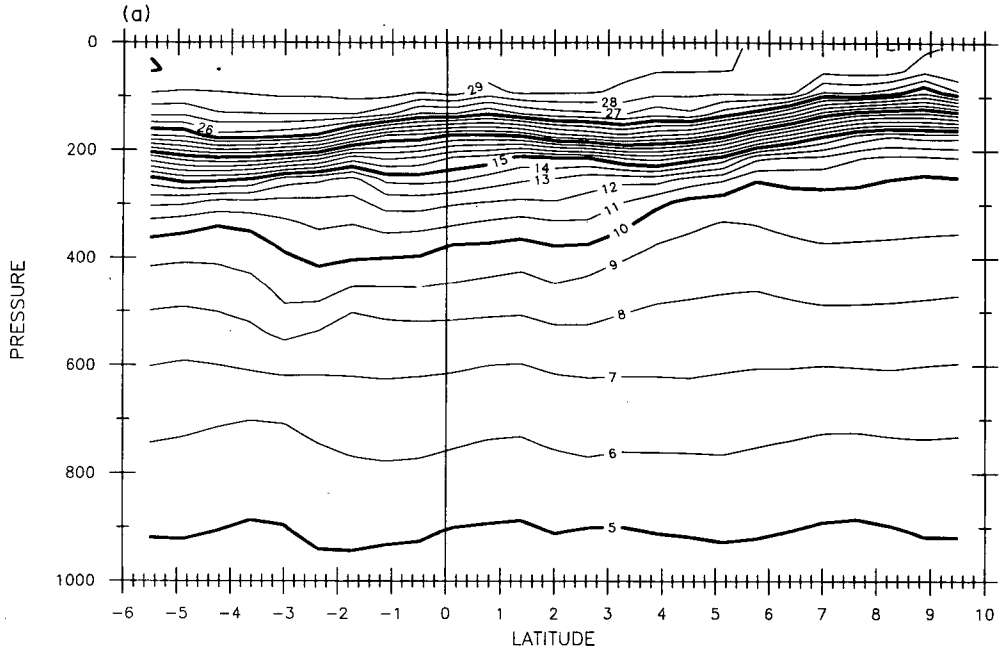
(a)
PRESSURE
LATITUDE
0
200
400
600
800
1000
−6 −5 −4 −3 −2 −1 0 1 2 3 4 5 6 7 8 9 10
29
28
27
26
15
14
13
12
11
10
9
8
7
6
5

Fig. 4a.

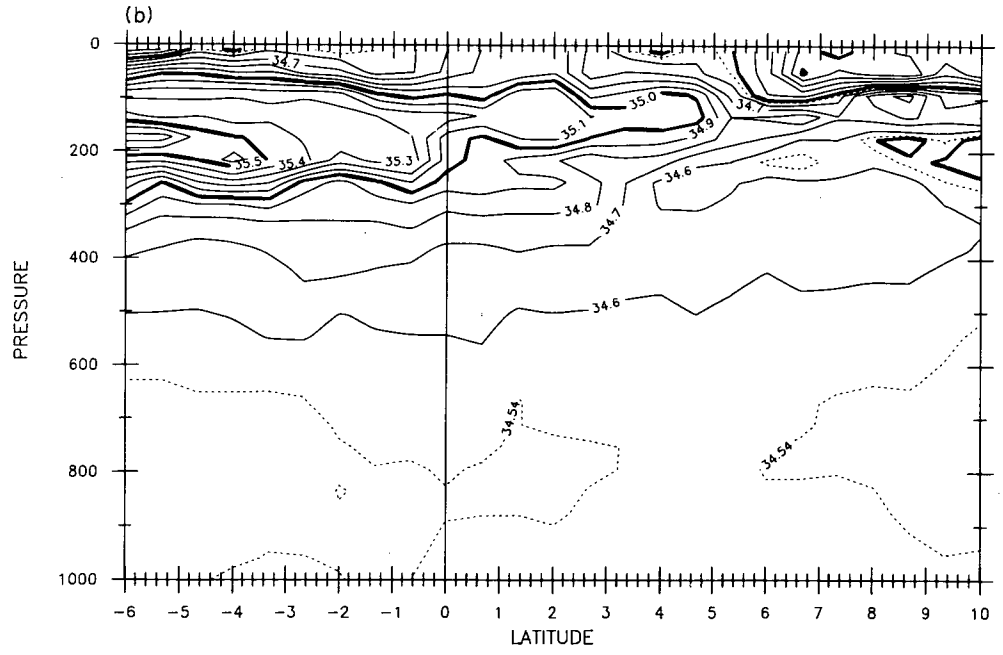
(b)
PRESSURE
LATITUDE
0
200
400
600
800
1000
−6 −5 −4 −3 −2 −1 0 1 2 3 4 5 6 7 8 9 10
34.7
35.0
34.9
35.1
35.5
35.4
35.3
34.6
34.8
34.7
34.6
34.54
34.54

Fig. 4b.

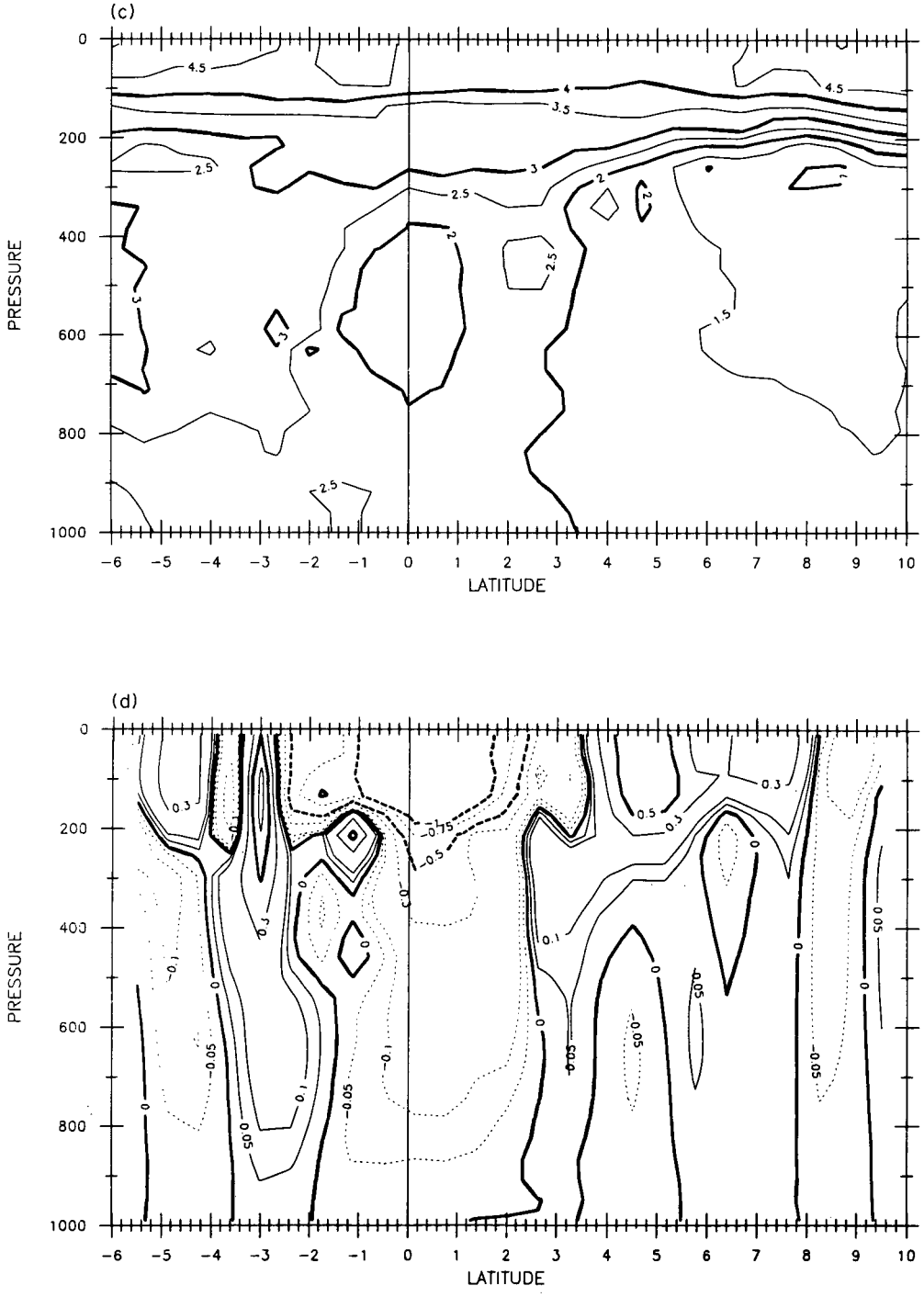

Fig. 4. Sections of (a) temperature in °C, (b) salinity in psu, (c) dissolved oxygen in ml l^{-1} and (d) zonal geostrophic velocity in m s^{-1} constructed from data obtained along 165°E during the first cruise of the US/PRC cooperative program.

Table 3. A summary of geostrophic current transports (in Sverdrups) relative to 1000 db *observed in* 1986 *for waters warmer than* 12°C. *Current boundaries, also given, mark the spatial extent of unidirectional flow in each current over which transport integrations were performed. Positive transports are east and north respectively*

	Cruise 1 Jan–Feb	Cruise 2 Nov–Dec
NECC (165°E)	32.0 (4°–8°N)	48.3 (1.5°–8°N)
NECC (141°30′E)	9.9* (4°–5°N)	31.7 (2°–6°N)
NEC (130°E)	–49.1 (7°–18°20′N)	–46.9 (8°–18°20′N)
Mindanao (10°N)	–	–16.6* (126°30′–130°E)
Kuroshio (18°20′N)	–1.7* (125°–130°E)	5.2* (123°–130°E)

* Section does not span the current's horizontal extent.

strong westward surface flow is indicated equatorward of ±4° latitude. Relative speeds in the NECC approach 75 cm s^{-1} around 5°N. Despite its limited latitudinal extent, NECC transport of water warmer than 12°C is 32 Sv (Table 3), greatly exceeding the annual mean value for area C (24 Sv). The northern SSCC was merged with the NECC on the section, NSSCC speed exceeds 10 cm s^{-1}. The southern SSCC also appears joined to an eastward surface flow, but as this surface current is only defined by one station pair this may simply reflect high frequency ageostrophic thermocline displacement.

A well-defined eastward surface flow is observed poleward of 4°S where surface speeds exceed 30 cm s^{-1}. This feature is closer to the equator than is typical for the SECC. Within 4° of the equator, the only area of eastward flow is centered at 250 db and 1°S. The swelling of the thermocline noted earlier is responsible for this feature. Geostrophically computed currents at and near the equator on instantaneous sections are highly uncertain (i.e. DELCROIX *et al.*, 1987). Direct velocity measurements at the equator during this period were in fact eastward in the thermocline at order 0.5 m s^{-1} (B. TAFT and M. MCPHADEN, personal communication).

141°30′E *and* 5°N *sections.* A short section was occupied between the equator and 5°N at 141°30′E longitude on cruise 1. The water mass characteristics observed here are very similar to those to the east. Significant differences in pycnocline structure are found, which are reflected in dynamic height (Fig. 5). These differences are discussed below where comparison is made with a nearly contemporaneous section on 165°E.

The stations made along 5°N sampled water mass characteristics which are similar to those found at 141°30′ and 130°E at this latitude. The deep oxygen field (below 400 db) exhibits elevated levels to the west [consistent with REID's (1965) map showing a tongue of relatively high oxygen extending northward along the western boundary]. No consistent direction to the geostrophic flow field is observed along the track.

130°E *and* 18°20′N *sections.* A section across the NEC was obtained late in cruise 1 along 130°E (Fig. 6), followed by a zonal section between 130° and 125°E. The NEC–NECC boundary on the 130°E section is somewhat confused due to the presence of cold-core eddies centered near 7° and 11°N. The overall minimum 0/1000 db dynamic height occurs at 7°N. Surface temperature on the section falls below 26°C poleward of 13°N; temperatures are somewhat colder than on the historical December–January–February

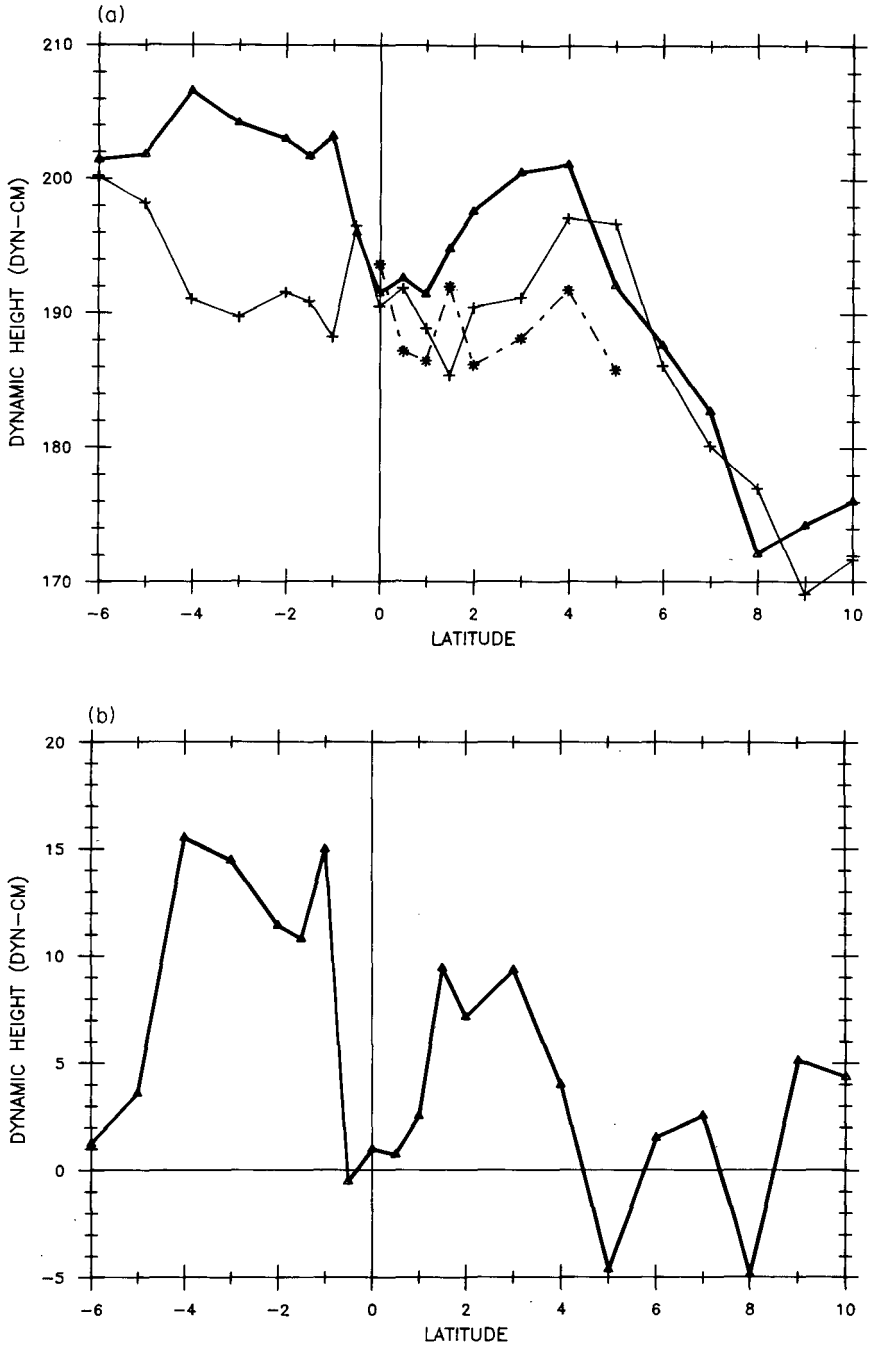

Fig. 5. (a) The meridional variation of surface dynamic height relative to 1000 db observed along 165°E (bold line) and 141°30′E (dashed line) on cruise 1. Also given are the dynamic height data along 165°E obtained on a cruise of the R.V. *Coriolis* which occurred 2 weeks prior to the US/PRC occupation of the section. (b) The 0/1000 db dynamic height difference between the two nearly contemporaneous sections collected on 165°E.

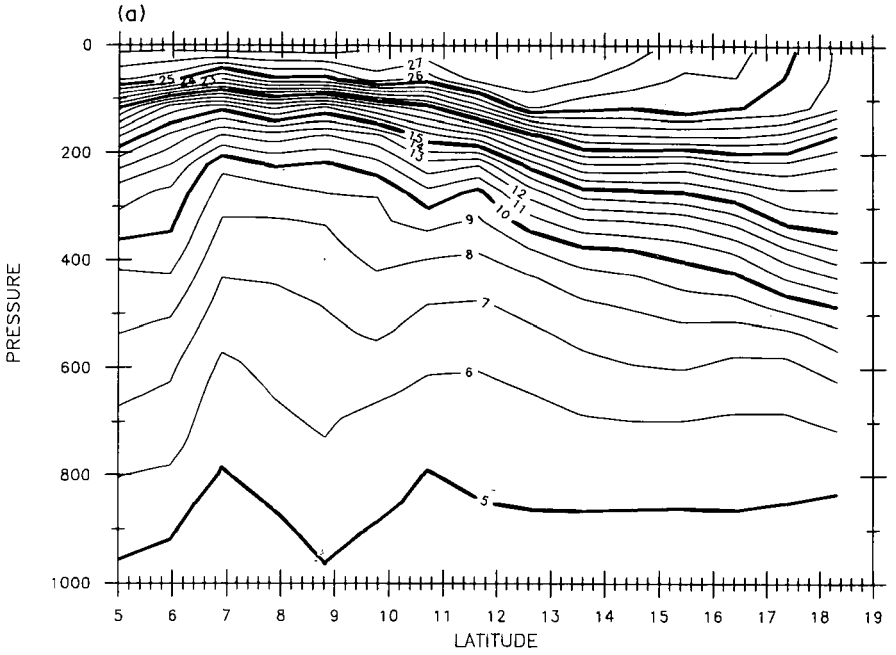
(a)
PRESSURE
0
200
400
600
800
1000
5 6 7 8 9 10 11 12 13 14 15 16 17 18 19
LATITUDE
27
26
25
15
13
12
11
10
9
8
7
6
5

Fig. 6a.

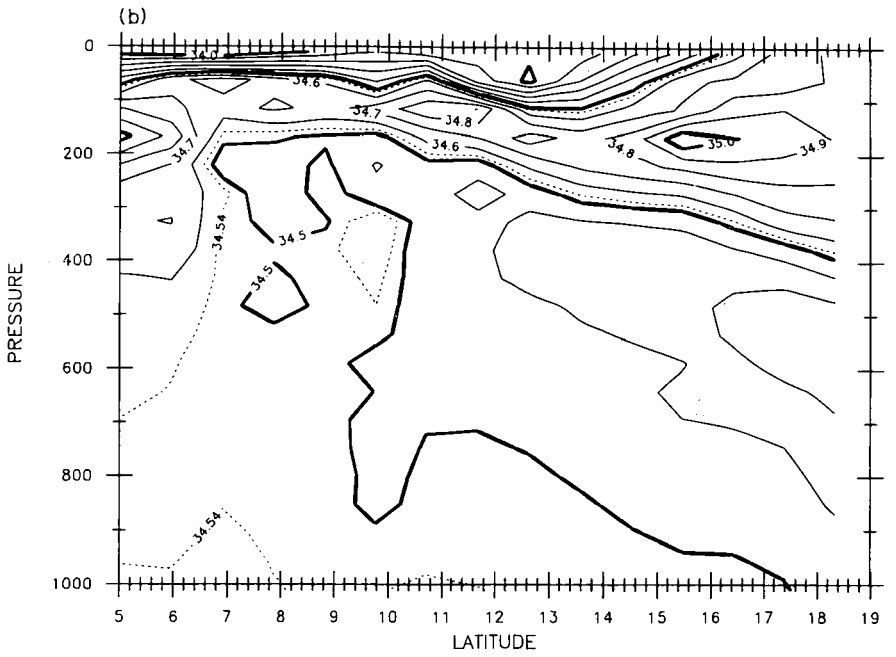
(b)
PRESSURE
0
200
400
600
800
1000
5 6 7 8 9 10 11 12 13 14 15 16 17 18 19
LATITUDE
34.6
34.7
34.8
34.6
34.7
34.8
35.0
34.9
34.54
34.5
34.5
34.54

Fig. 6b.

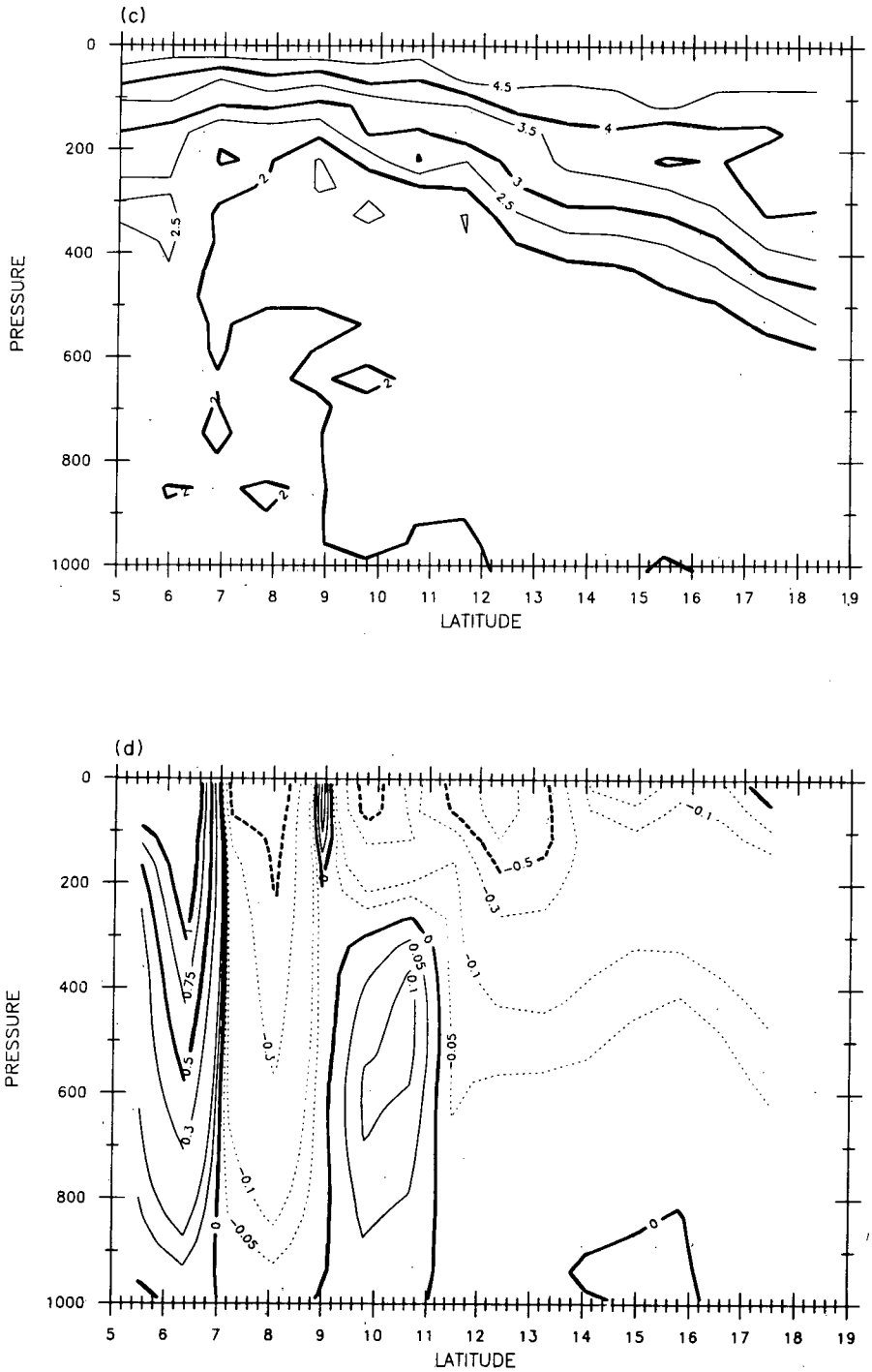

Fig. 6. Sections of (a) temperature in °C, (b) salinity in psu, (c) dissolved oxygen in ml l^{-1} and (d) zonal geostrophic velocity in m s^{-1} constructed from data obtained along 130°E during the first cruise of the US/PRC cooperative program.

section A. The northern hemisphere salinity maximum is well resolved, achieving values of 35.0 at 17°N. This feature is associated with a relative oxygen maximum in depth (REID, 1965). The lowest values in the salinity maximum on the section occur around 9°N where values just under 34.7 are found. This feature appears at 7°N in the annual mean section A, a discrepancy perhaps related to the presence of eddies. Also prominent on the section is the tongue of NPIW; as in the annual mean, core salinities fall below 34.3 near 20°N.

The zonal geostrophic velocity field is somewhat more structured than the mean section of area A, again due to the eddy field. The southernmost eddy appears to reinforce the east–west velocity difference between the NEC and NECC; speeds exceed 100 cm s^{-1} (eastward) in the south and 75 cm s^{-1} (westward) on the northern flank of the eddy. Strong westward flow is also seen on the northern flank of the eddy at 11°N. The southern flank shows a local minimum in surface westward current with eastward directed flow at depth. An estimate of NEC transport ($T > 12$°C) was obtained by integrating the velocity field between 7°N and 18°20′N (Table 3). The result of –49.1 Sv is larger than the historical mean, in part because the 7°N eddy transport is included in the estimate.

The zonal section at 18°20′N was a disappointment, as the section did not extend far enough west to sample the Kuroshio flow at the Philippine coast. The water mass properties on the section closely resemble those found at the northern end of the 130°E section with virtually no horizontal gradients. Net meridional transport through the section is 1.7 Sv to the south. This finding is consistent with the historical data analysis which indicates the Kuroshio is a narrow feature.

Comparison with Surtropac 5. Roughly 2 weeks prior to cruise 1 sampling along 165°E, the section was occupied by the R.V. *Coriolis* working out of Noumea, New Caledonia (T. DELCROIX, personal communication). The Coriolis sampling began at 20°S on 10 January 1986, reaching 6°S on 15 January and 10°N on 21 January. Cruise 1 re-occupied the 10°N site on 30 January and reached 6°S on 5 February. A striking change in the upper ocean density field took place over this short interval which is reflected in dynamic height (Fig. 5). Between 1° and 4° latitude (north and south) the thermocline fell between the two cruises, 0/1000 db dynamic height increased a maximum of 15 dyn-cm. Near the equator little change in surface dynamic height is found; however, downward displacements of isotherms below the thermocline of order 50 m are observed. At the time of the US/PRC cruise, the perturbation did not extend west to the 141°30′E section; dynamic height there is similar in magnitude and structure to the Surtropac 5 observations. The sense of the dynamic height changes are for increased westward geostrophic flow near the equator and enhanced eastward flow poleward of 4° latitude on the US/PRC cruise.

Cruise 2: *November–December* 1986

165°E *section.* The surface properties observed along 165°E in November–December 1986 differ significantly from those sampled 11 months earlier (Fig. 7). Within 3° of the equator, mean surface temperature is 0.7°C cooler and surface salinity is 0.4 lower on cruise 2 than on cruise 1. The horizontal structure of the subsurface water mass cores are similar on the two cruises (e.g. the salinity maximum core values and latitudinal extent are virtually identical), however the thermocline depth structure and hence relative geostrophic flow are quite distinct. Whereas cruise 1 sampled strong westward flow on the section,

cruise 2 is dominated by eastward currents. The southern extremity of the NEC is seen poleward of 8°N with westward speed of 10 cm s^{-1} or less. Surface eastward flow is indicated to the south nearly continuously to 7°S. NECC speeds above 50 cm s^{-1} are seen between 4° and 7°N, a narrow band of eastward flow is also found at 2°N and is indicated at 1–2°S. Farther south, eastward speeds consistently attain values of 10 cm s^{-1}. A band of

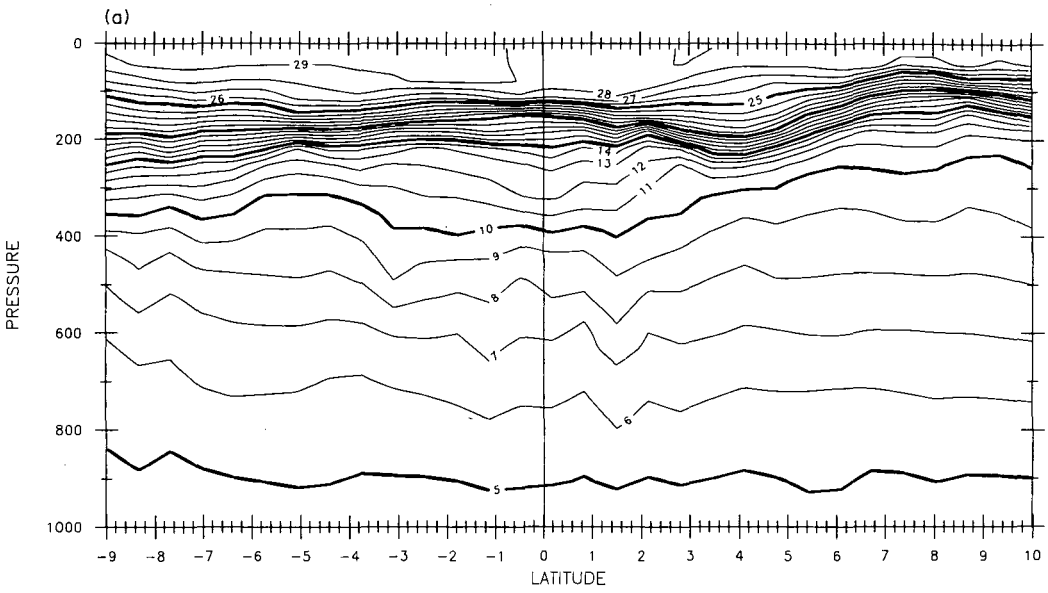

Fig. 7a.

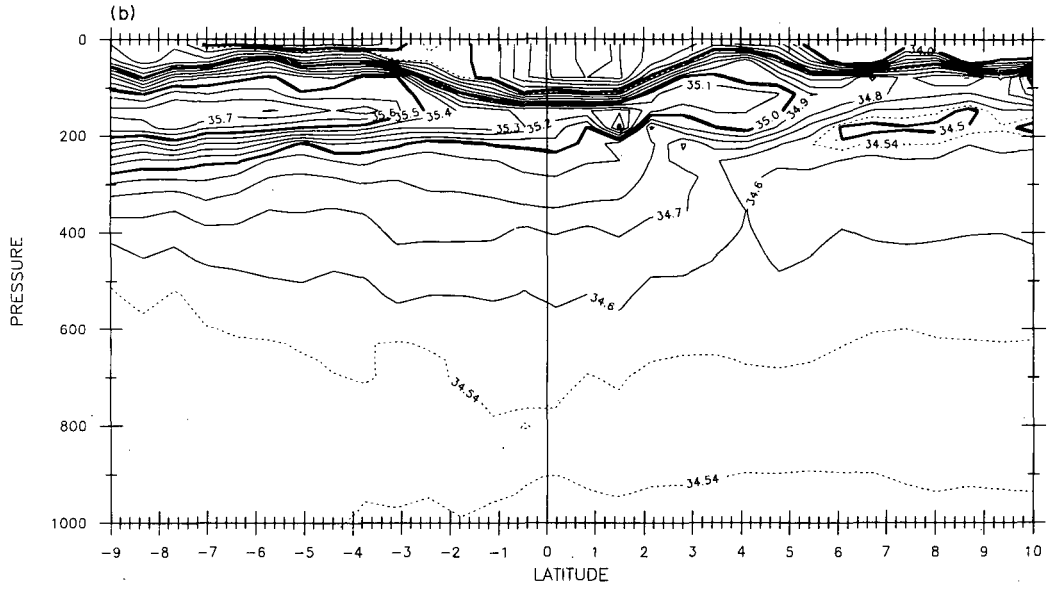

Fig. 7b.

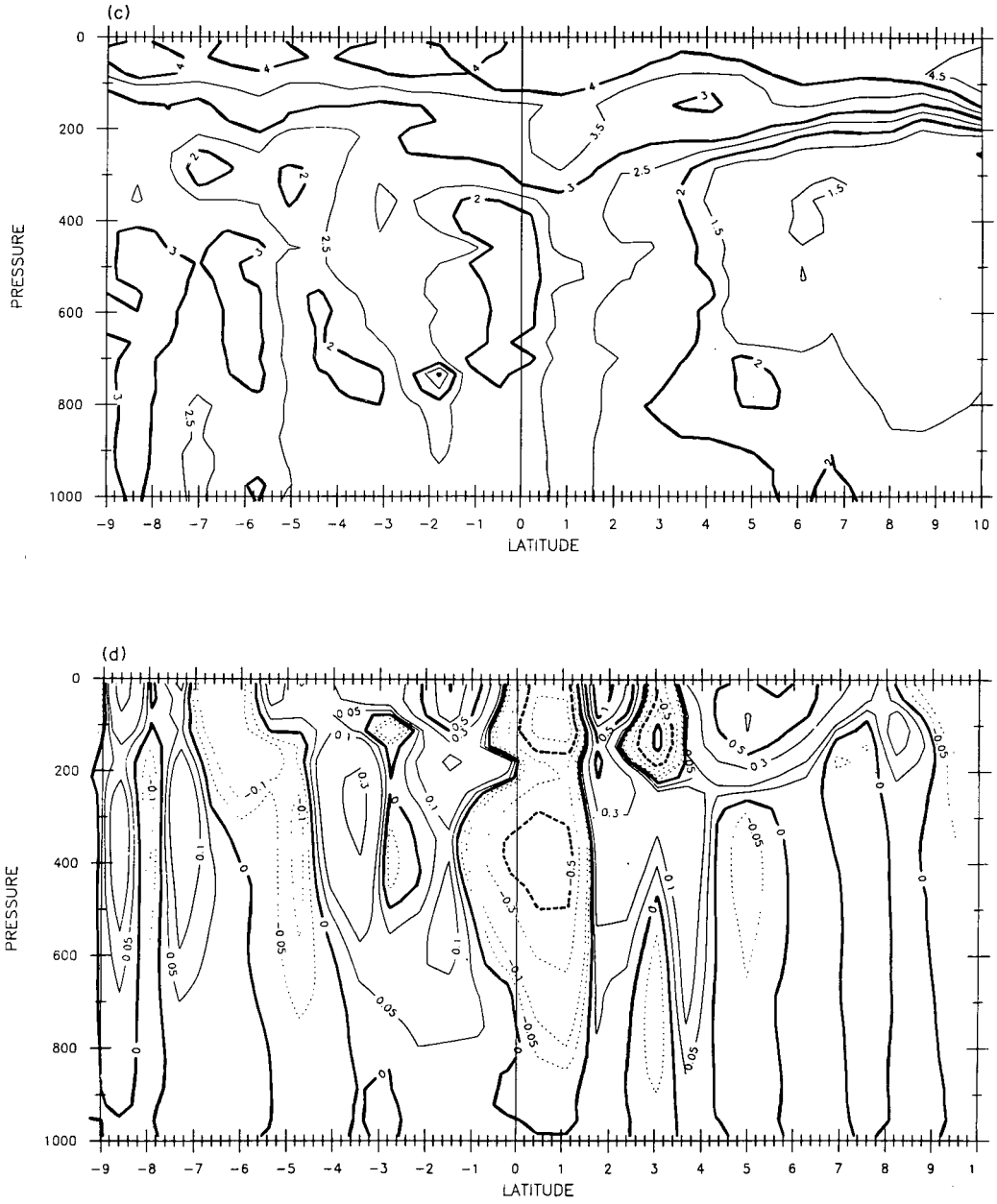

Fig. 7. Sections of (a) temperature in °C, (b) salinity in psu, (c) dissolved oxygen in ml l^{-1} and (d) zonal geostrophic velocity in m s^{-1} constructed from data obtained along 165°E during the second cruise of the US/PRC cooperative program.

westward flow is indicated between 6° and 7°S and a spatially oscillatory pattern, at the scale of the station spacing, is obtained near the Solomon Islands.

Subsurface flow is also strongly eastward. The major exception to this is the EIC at 400 db about the equator. The dynamic height curvature estimator at the equator yields a subsurface eastward velocity extremum in the thermocline. Westward geostrophic surface flow is also obtained; however, surface drifters deployed at the equator on cruise 2 traveled east at 50 cm s^{-1} or more (D. HANSEN, person communication), suggesting again that the equatorial geostrophic calculation is not reliable for the surface flows.

NECC transport estimates were obtained by integrating the zonal velocity field down to the 12°C isotherm (Table 3). Between 3° and 8°N an eastward transport of 36.1 Sv is obtained. Extending the integration to 1.5 N yields a transport of 48.3 Sv. Both figures are larger than the NECC transport value obtained from the cruise 1 data and greatly exceed the annual and December–January–February season mean transports evaluated for this area. Net warm water transport between 1° and 9.5°S is found to be eastward at 19.0 Sv. Anomalous eastward transport at this time could reflect the onset conditions of the 1986–1987 ENSO event.

141°30′E *section.* A second crossing of the NECC and near equatorial zone was obtained at 141°30′E on cruise 2 (Fig. 8). The density and velocity fields indicate that an anticyclonic eddy was crossed at the northern end of the section (eddy appears centered near 7°N). Eastward relative flow is seen north of 7°N with a band of westward flow between 6° and 7°N. Strong NECC surface velocities, in excess of 75 cm s^{-1} are estimated for the area south of 6°N with eastward surface flow extending to 2°N. Net surface water transport between 2° and 6°N is estimated to be 31.7 Sv, essentially identical to the December–January–February season and annual mean transports computed from the historical data. The NSSCC is centered between 3° and 4°N on the section, connected vertically with the surface NECC flow and horizontally at 200–300 m with the EUC. The EUC signature in the density field is quite strong on this crossing, yielding a well-developed eastward jet in the calculated velocity section. No indication of the EIC is seen in the velocity section, however, low oxygen is again found on the equator at 400–700 m depth.

The surface flow south of 2°N is predominantly westward (the only indication of eastward surface flow is at the equator where the geostrophically computed velocity is unreliable). Thus, as was the case on the first cruise, the flow fields at 141°30′ and 165°E sampled on cruise 2 are dramatically different; the eastward flow event observed at 165°E had not extended west to 141°30′ at the time of cruise 2.

Particularly well-developed westward flow is seen south of the equator. Here, adjacent to the Papua New Guinea coast, the highest southern subtropical water salinity and lowest AAIW salinity are found consistent with the WEPOCS discovery of westward subsurface flow along this coast. Its' observation here supports the WEPOCS investigators' contention that this flow is a permanent feature of the circulation of the region. The SSSCC is not observed at this longitude: no doubt because of the geometry of the area (proximity of the Papua New Guinea coast to the equator). Net surface water transport to the west is computed between 1° and 2°S at –10.4 Sv with transport weighted temperature and salinity of 22.15°C and 35.00 psu. As the section terminated 30 nmi from the coast, this likely represents an underestimate of the westward transport. Note that the presence of strong flow at depth leads to a relatively colder mean temperature for the flow than that obtained from the historical data analysis (Table 1).

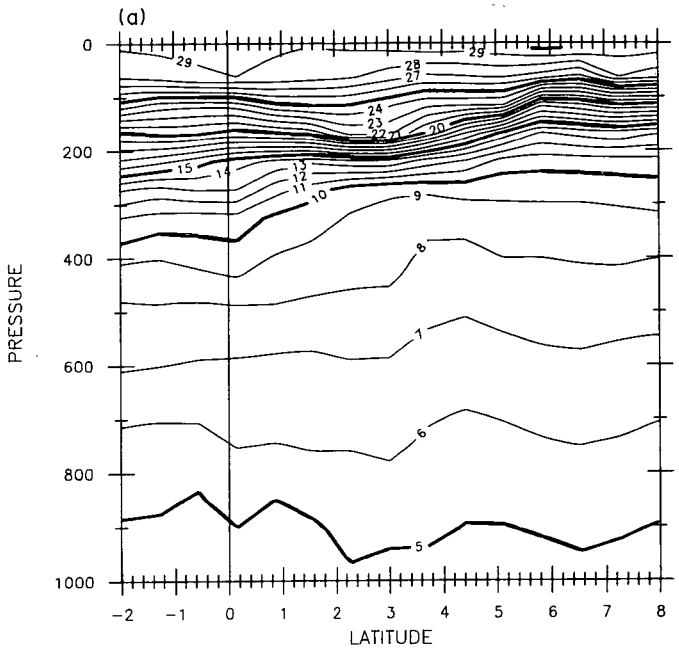
(a)
PRESSURE
LATITUDE
0
200
400
600
800
1000
−2 −1 0 1 2 3 4 5 6 7 8
29
28
27
24
23
22.71
20
15
14
13
12
11
10
9
8
7
6
5

Fig. 8a.

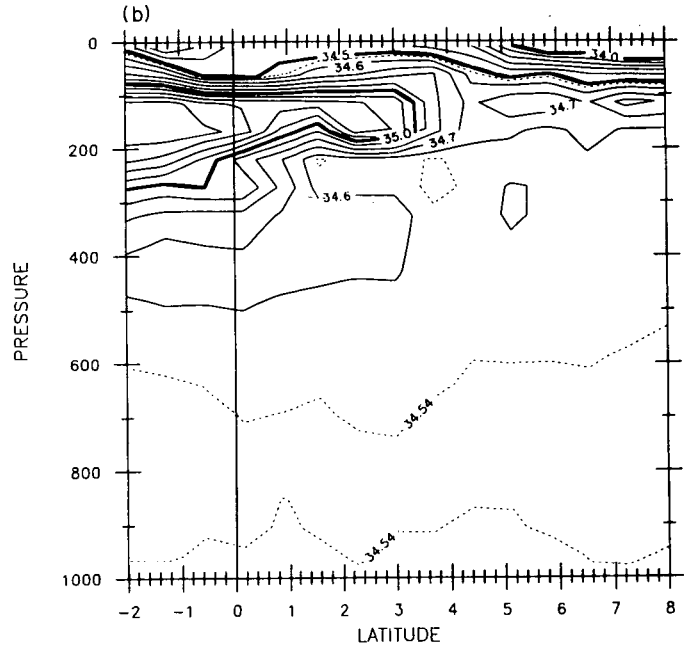
(b)
PRESSURE
LATITUDE
0
200
400
600
800
1000
−2 −1 0 1 2 3 4 5 6 7 8
34.5
34.6
34.0
34.7
35.0
34.7
34.6
34.54
34.54

Fig. 8b.

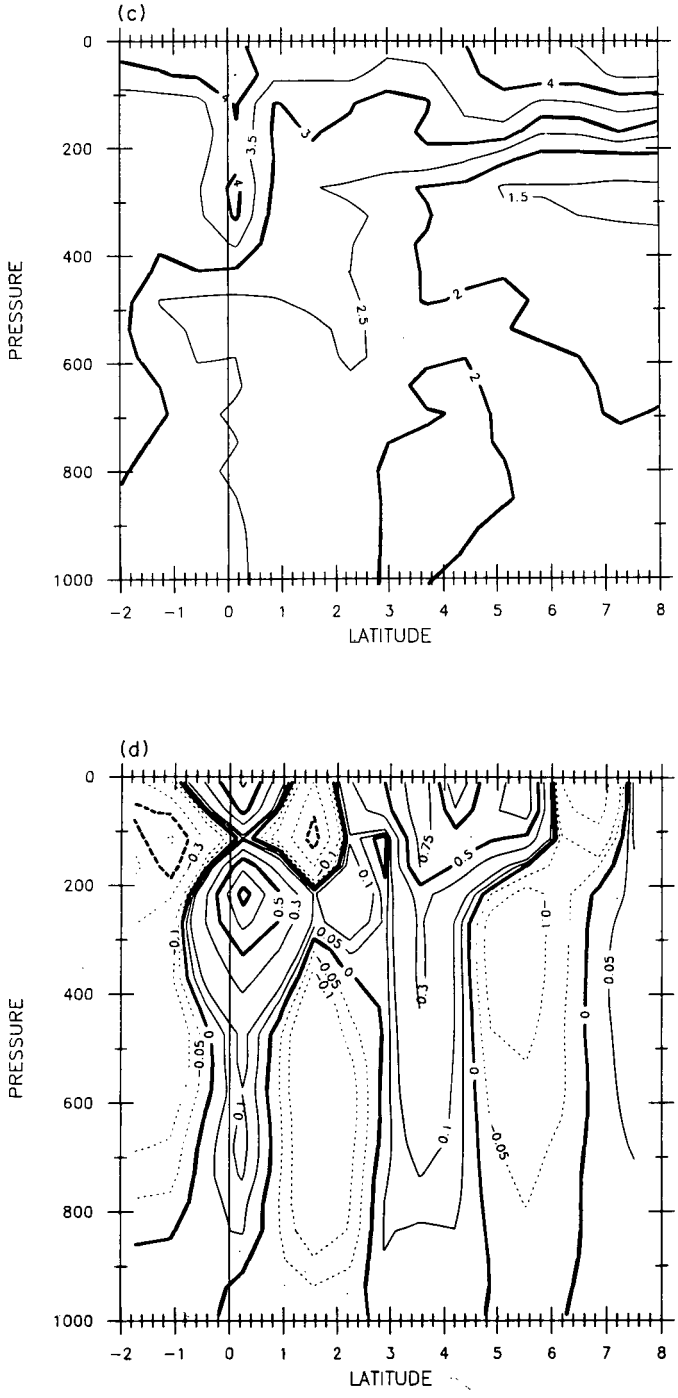

Fig. 8. Sections of (a) temperature in °C, (b) salinity in psu, (c) dissolved oxygen in ml l^{-1} and (d) zonal geostrophic velocity in m s^{-1} constructed from data obtained along 141°30′E during the second cruise of the US/PRC cooperative program.

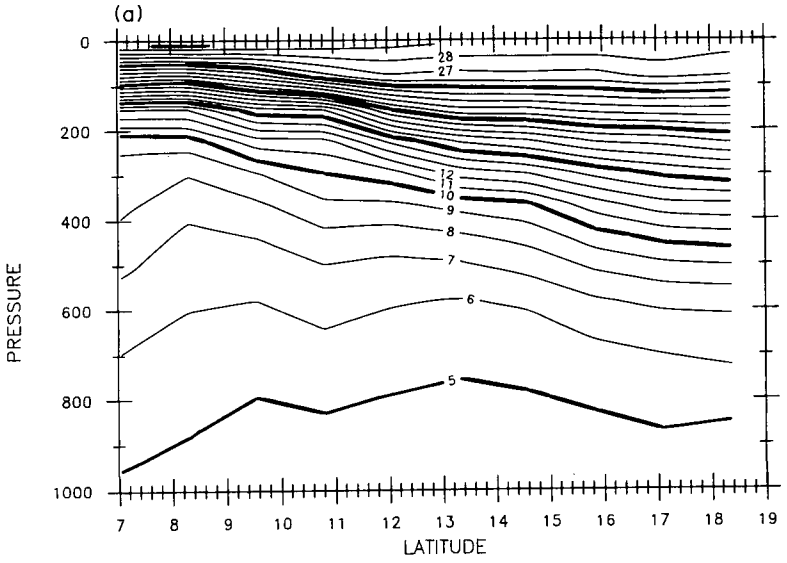
(a)
0
200
400
600
800
1000
PRESSURE
28
27
12
11
10
9
8
7
6
5
7 8 9 10 11 12 13 14 15 16 17 18 19
LATITUDE

Fig. 9a.

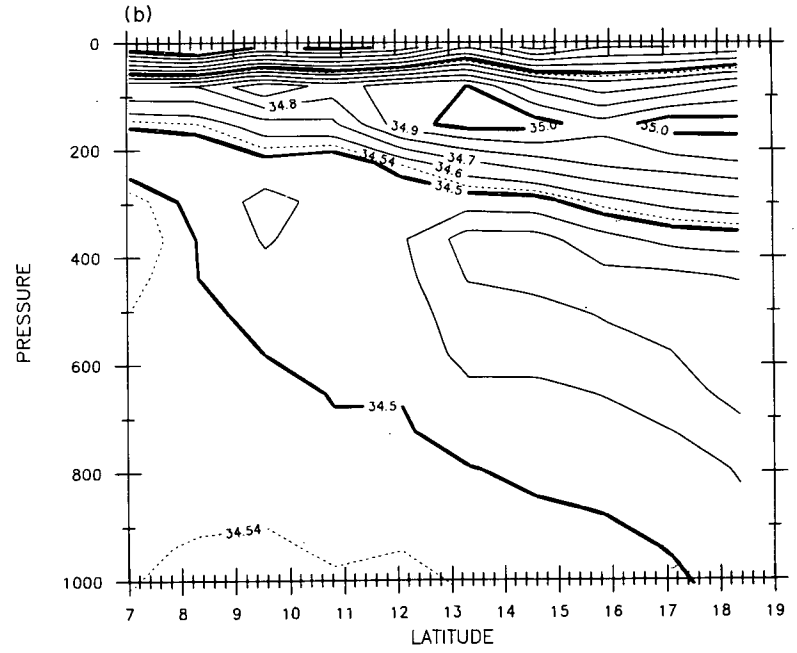
(b)
0
200
400
600
800
1000
PRESSURE
34.8
34.9
35.0
35.0
34.54
34.7
34.6
34.5
34.5
34.54
7 8 9 10 11 12 13 14 15 16 17 18 19
LATITUDE

Fig. 9b.

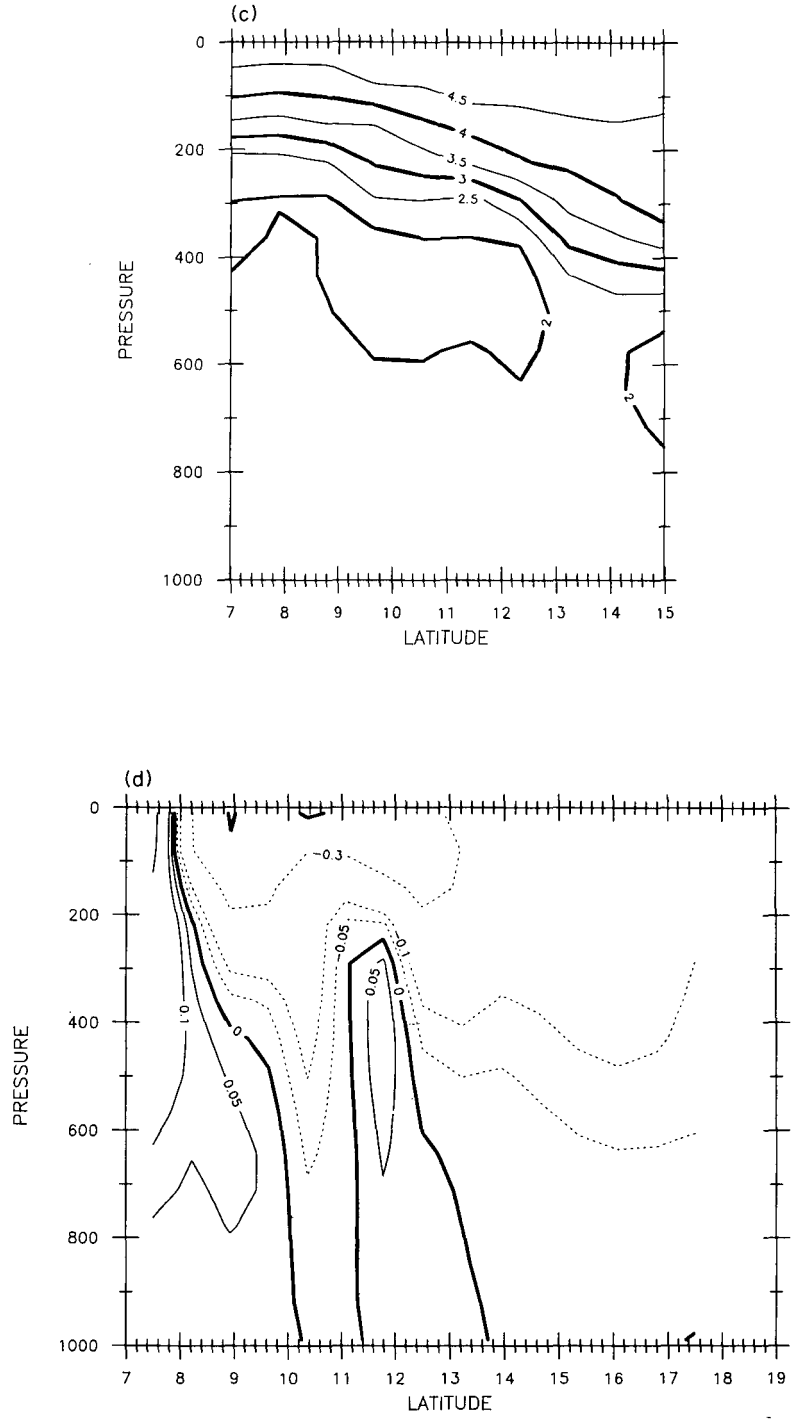

Fig. 9. Sections of (a) temperature in °C, (b) salinity in psu, (c) dissolved oxygen in ml l^{-1} and (d) zonal geostrophic velocity in m s^{-1} constructed from data obtained along 130°E during the second cruise of the US/PRC cooperative program.

Zonal section along 7°–10°N. Station work was conducted between 141°30′ and 130°E along 7°N, roughly paralleling the boundary between the NEC and NECC. Meridional flow relative to 1000 db is everywhere weak along the track; speeds are less than 5 cm s^{-1} and alternate sign in the horizontal. Somewhat lower salinity water at the level of the shallow minimum is observed in the west accompanied by higher dissolved oxygen content. As observed in cruise 1, higher oxygen at the deep salinity minimum levels are found in the west.

Continuing west, stations were occupied along 10°N west of 130°E and terminated 30 nmi from the Philippine coast. As was the case in the historical area E data, the thermocline deepens fairly smoothly to the west along the section. Strongest horizontal gradients are seen near the boundary. Salinity at the salinity maximum is largest at the ends of the section but higher oxygen levels are observed near the coast, consistent with a boundary flow carrying fluid from farther north. The shallow salinity minimum attains lowest values near the coast. Southward flow relative to 1000 db is found west of 130°E with a net warm water transport of –16.6 Sv, close to the annual mean estimate of –17.5 (recall, both are likely underestimates). Transport weighted mean temperature and salinity are 23.18°C and 34.61, respectively, both slightly greater than the estimates made with the historical data.

The 130°E *and* 18°20′N *sections.* The eddy field is not as pronounced on the cruise 2 130°E section as on cruise 1 (Fig. 9). The dynamic height ridge between the NEC and NECC occurs at 8°N with surface speeds in the NEC exceeding 30 cm s^{-1} between 8° and 13°N. Somewhat higher salinities at the salinity maximum are observed on cruise 2 (isolated values above 35.0 are seen to 11°N) while the NPIW tongue appears to extend farther to the south (the 34.3 isohaline reaches 12°N as compared to 16°N on cruise 1). NEC warm water transport integrated between 8° and 18°20′N is –46.9 Sv, comparable to the historical mean value.

The section along 18°20′N also was terminated 30 nmi from the coast and because of winch difficulties and typhoons, consists of a limited number of irregularly spaced stations. Dynamic height difference (0/1000 db) between the shoreward station and 130°E is only 10.5 dyn-cm and net northward warm water transport is just 5.2 Sv.

4. DISCUSSION AND CONCLUSIONS

The historical data analysis indicated a substantial contribution of southern hemisphere water to the mean NECC, a finding somewhat at odds with recent transient tracer studies (e.g. FINE *et al.*, 1988). In the central and eastern Pacific, a tritium front is found at the southern boundary of the NECC dividing waters with high load in the north from low values in the SEC. At these longitudes then, the NECC appears comprised of northern hemisphere water. The western Pacific may be different in that the NECC is found closer to the equator than in the east. In the mean, waters with southern hemisphere characteristics may move east with the NECC part way across the basin, then turn south and recirculate back west somewhere west of the date line. Some indication of this is seen in the historical data where the NECC volume transport decreases between areas B and C mostly due to losses in the southern part of the current.

Low latitude flow adjacent to the Philippine–Papua New Guinea–Solomon Islands coast appears central to the circulation and water mass budgets of the western Pacific. Inclusion of the coastal flow adjacent to Papua New Guinea could significantly alter the heat budget estimate made in Section 2. The presence of strong subsurface flow leads to a

reduced transport weighted mean temperature for the southern hemisphere westward flow as compared to that obtained from the historical data. Using the cruise 2 mean temperature of 22.15°C for T_{sec} in equation (5) results in a net heat flux divergence for the far western corner of the study region, –33.9° C Sv. [Note that the assumed value of S_{sec} in equation (3) is in fact close to that obtained on cruise 2, 35.1 vs 35.0.] This heat budget result translates for steady state into a net ocean heat gain from the atmosphere of order 100 W m^{-2}, in somewhat better agreement with the figures obtained from bulk aerodynamic calculations.

The present results also confirm the WEPOCS finding of subsurface westward flow at the Papua New Guinea coast transporting saline low oxygen southern hemisphere subtropical water and relatively fresh, well-oxygenated AAIW northwestward. The eventual fate of these waters is not known. The present water mass budget indicates that part of the flow turns back to the east with the NECC. The deeper flow may proceed north to cross the equator and account for the relatively high oxygen levels found near the Philippine coast.

Comparison of the re-occupied sections from the first US/PRC cruise and the R.V. *Coriolis* section dramatizes the magnitude of high frequency variability of the tropical upper ocean density field. Subsequent analysis of these observations will, by necessity, involve joint analysis with continuous records from moorings and islands to try and sort out the time scales of the variability. This will be particularly interesting for the data obtained in the 1986–1987 period during the onset stage of the 1986–1987 El Niño–Southern Oscillation event.

Acknowledgements—Our analysis of the historical data was aided greatly by M. Woodgate-Jones. Collection of the modern data was accomplished by a team of investigators, technicians and marine personnel from the United States and the People's Republic of China. Without their efforts the two high quality data sets would not have been acquired. We wish, in particular, to acknowledge the efforts of M. Francis in the collection and processing of the CTD data and the sea-going personnel from both countries. We also thank T. Delcroix, M. McPhaden and B. Taft for sharing data with us prior to its publication. This work was supported by grant no. NA85AA-D-AC117 from the Tropical Ocean Global Atmosphere program of the National Oceanic and Atmospheric Adminstration to the Woods Hole Oceanographic Institution. Woods Hole Oceanographic Contribution no. 6553.

REFERENCES

BAUMGARTNER A. and E. REICHEL (1975) *The World water balance mean annual global continental and marine precipitation, evaporation and run off.* Elsevier, New York, 179 pp.

DELCROIX T. and C. HENIN (1988) Observations of the Equatorial Intermediate Current in the western Pacific Ocean (165 E). *Journal of Physical Oceanography*, **18**, 363–366.

DELCROIX T., G. ELDIN and C. HENIN (1987) Upper ocean water masses and transports in the western tropical Pacific (165 E). *Journal of Physical Oceanography*, **17**, 2248–2261.

FINE R. A. (1985) Direct evidence using tritium data for the throughflow from the Pacific to the Indian Ocean. *Nature*, **315**, 478–480.

FINE R. A., W. H. PETERSON and H. G. OSTLUND (1987) The penetration of tritium into the tropical Pacific. *Journal of Physical Oceanography*, **17**, 553–564.

GORDON A. L. (1986) Interocean exchange of thermocline water. *Journal of Geophysical Research*, **91**, 5037–5046.

HAYES S. P. (1982) A comparison of geostrophic and measured velocities in the Equatorial Undercurrent. *Journal of Marine Research*, **40** (Suppl.), 219–229.

HAYES S. P., J. M. TOOLE and L. J. MANGUM (1983) Water-mass and transport variability at 110 W in the equatorial Pacific. *Journal of Physical Oceanography*, **13**, 153–168.

HELLERMAN S. and M. ROSENSTEIN (1983) Normal monthly wind stress over the world ocean with error estimates. *Journal of Physical Oceanography*, **32**, 1093–1104.

HISARD R., J. MERLE and B. VOITURIEZ (1970) The Equatorial Undercurrent at 170 E in March/April 1967. *Journal of Marine Research*, **28**, 281–303.
KENDALL T. R. (1969) Net transports in the western equatorial Pacific Ocean. *Journal of Geophysical Research*, **74**, 1388–1396.
LINDSTROM E., R. LUKAS, R. FINE, E. FIRING, S. GODFREY, G. MEYERS and M. TSUCHIYA (1987) The Western Pacific Ocean Circulation Study (WEPOCS). *Nature*, **330**, 553–557.
LAMONTAGNE G., M. FRANCIS, L. MANGUM, Z. WONG, S. PU, R. MILLARD and J. TOOLE (1988) CTD/O_2 observations from the United States/People's Republic of China cooperative program in the western equatorial Pacific Ocean: Cruise 1 Jan–Feb 1986, Cruise 2 Nov–Dec 1986. WHOI Tech. Report, in preparation.
MAGNIER Y., H. ROTSCHI, P. RUAL and C. COLIN (1973) Equatorial circulation in the western Pacific. *Progress in Oceanography*, **6**, 29–46.
MASUZAWA J. (1964) Flux and water characteristics of the Pacific North Equatorial Current. In: *Studies on oceanography* (dedicated to Prof. Hidaka in commemoration of his 60th birthday), Tokyo, pp. 121–128.
MASUZAWA K. (1972) Gross hydrographic features of the western north Pacific. In: *Kuroshio, physical aspects of the Japan current*, H. STOMMEL and K. YOSHIDA, editors, University of Washington Press, pp. 97–116.
MILLARD R. C. (1982) CTD calibration and data processing techniques using the 1978 practical salinity scale. International STD conference and workshop proceedings.
NITANI H. (1972) Beginning of the Kuroshio. In: *Kuroshio, physical aspects of the Japan current*, H. STOMMEL and K. YOSHIDA, editors, University of Washington Press, pp. 129–163.
PIOLA A. R. and A. L. GORDON (1984) Pacific and Indian Ocean upper layer salinity budget. *Journal of Physical Oceanography*, **14**, 747–753.
REID J. L. (1965) Intermediate water of the Pacific Ocean. *John Hopkins Oceanographic Studies* 2, 85 pp.
SVERDRUP H. U. (1947) Wind-driven currents in a baroclinic ocean, with application to the equatorial currents of the eastern Pacific. *Proceedings of the National Academy of Science, U.S.A.*, **33**, 318–326.
TSUCHIYA M. (1968) Upper waters of the Intertropical Pacific Ocean. *John Hopkins Oceanographic Studies* 4, 50 pp.
TSUCHIYA M. (1975) subsurface countercurrent in the Pacific Ocean. *Journal of Marine Research*, **33** (Suppl.), 145–175.
TSUCHIYA M. (1982) On the Pacific upper-water circulation. *Journal of Marine Research*, **40** (Suppl.), 777–799.
WANG Z., C. MA and E. ZOU (1983) The interannual variation of the western Pacific water mass characteristics and its relation to other factors. *Journal of Oceanography of Huanghai and Bohai Seas*, **1**, 12–26.
WEARE B. C., P. T. STRUB and M. D. SAMUEL (1981) Annual mean surface heat fluxes in the tropical Pacific Ocean. *Journal of Physical Oceanography*, **11**, 705–717.
WRYTKI K. (1961) Physical oceanography of the southeast Asian waters. NAGA Report 2, University of California, SIO, 195 pp.

APPENDIX

Data processing and analysis procedures

NODC data. The historical data analysis focused on the hydrographic temperature and salinity observations archived at the National Ocean Data Center. Hydrographic casts from the western Pacific study area which extended deeper than 500 m were obtained (Fig. 1) and an initial survey of the data base was conducted. The observations spanned the time period of 1906–1981, the bulk of the measurements were taken after 1965. Data coverage was sparse in general, somewhat more so in the boreal autumn season. No obvious bias in sampling density associated with El Niño–Southern Oscillation events was apparent. Of those hydrocasts obtained, the bulk extended to 1000 db. While deeper observations were available at some locations and times, the present study was restricted to the upper 1000 db to optimize uniformity of the data base. For subsequent analysis, each station was gridded in depth to fixed levels by interpolation.

The hydrographic data were subdivided into five geographic regions labeled A–E (Fig. 1). Seasonal mean meridional temperature and salinity sections were constructed from the data in areas A, B and C by ensemble averaging in 2° latitude bins by season (where the winter season was defined as the December–January–February period). Estimates of the standard deviations of temperature and salinity at each depth obtained during the averaging process were used to edit the resulting mean profiles. (Erroneous mean data were identifiable by their elevated standard deviations relative to values in adjacent averaging bins.) Only 21 averaged profiles of the total of 148 required editing. A measure of the uncertainty in the seasonal mean temperature and salinity

profiles is afforded by the standard deviation information. At depths below the main thermocline, temperature and salinity standard deviations were 0.25°C and 0.075‰, respectively, based on typical ensembles of 25–50 stations. Dynamic height relative to 1000 db was estimated from the seasonal mean temperature and salinity profiles and baroclinic velocity computed between adjacent stations. Volume, temperature and salinity transports for waters warmer than 12°C were subsequently evaluated by summing contiguous station pair transports of uniformly directed flow. Values of transport weighted mean temperature and salinity for the currents were obtained by dividing the temperature and salinity transports by the respective volume transport for each current.

Uncertainty in the velocity can be evaluated from dynamic height standard deviation information also obtained during averaging. Ensemble mean dynamic height profiles and their standard deviations were evaluated from individual station dynamic height data. Typical surface dynamic height standard deviation relative to 1000 db was 10 dyn-cm, ranging from seven near the equator to 15 at latitudes poleward of 8°. Based on 25 independent profiles in each latitude bin and assuming adjacent bins are uncorrelated, a velocity uncertainty of order 10 cm s^{-1} across a distance of 200 km is obtained (at a latitude of 10°). This translates into a transport uncertainty of order 3 Sv (integrating vertically to 200 m depth).

Annual mean temperature and salinity sections were constructed by averaging the four seasonal sections, a procedure thought to reduce seasonal bias in the annual mean stemming from uneven sampling throughout the year. Dynamic height was computed from the annual mean temperature and salinity profiles; velocity and transports were estimated as described earlier.

Owing to the scarcity of observations in areas D and E, seasonal averaging was not deemed feasible. All available data were grouped into 1° longitude bins and ensemble averaged temperature and salinity profiles were obtained. The resulting sections are thus somewhat biased in time as few observations were available in the November–December–January period. Station editing and calculation of dynamic height and transports proceeded as before. We believe the 1° spatial resolution employed, while as dense as the data base permits, does not fully resolve the flow field adjacent to the western boundary. The expectation is that the Kuroshio and Mindanao Current transports are likely underestimated as a result. A similar caveat may be made regarding transport estimates along the Papua New Guinea coast.

CTD/O_2 *data.* CTD/O_2 observations were collected in the western equatorial Pacific on two recent cruises as part of a cooperative research program between the United States and the People's Republic of China. Sampling on cruise 1 occurred in January–February 1986 aboard R.V *Xiangyanghong* No. 14. Cruise 2 took place in November–December 1986 aboard *Xiangyanghong* No. 5. Station maps for both cruises appear in Fig. A1. NBIS/EG&G Mark III CTD/O_2 underwater units were employed on both cruises; water samples obtained from a GO 12 bottle rosette sampler were analysed for salinity and dissolved oxygen to provide calibration information for the CTD sensors. (Salinity calculated with these modern data are reported on the practical salinity scale.) As neither PRC vessel was capable of slow speed manoeuvring, stations were made while the ship lay hove-to, usually broadside to the prevailing winds. Consequently, wire angles were often extreme and station depth was limited by the 6000 m of conducting cable available on the winch. Nominal station depths were 2500 db; deep stations (pressure >3500 db) were obtained at seven sites on cruise 1 and 15 sites on cruise 2.

Data processing techniques follow those outlined by MILLARD (1982). Briefly, laboratory calibrations of the temperature, pressure and conductivity sensors were obtained in the United States before and after each field use of the instruments. These results established the calibrations of the pressure and temperature data obtained during the cruises (no thermometry conducted at sea). Water samples were analysed at sea for salinity and dissolved oxygen content to provide calibration information for the conductivity and oxygen cells. The salinity data are believed accurate to 0.002 psu while the oxygen uncertainty is 0.2 ml l^{-1}. Details of the CTD collection and calibration procedures are given by LAMONTAGNE *et al.* (1988).

The basic data set produced has 2 db vertical resolution. A condensed data set for analysis was constructed by vertically averaging the T, S and O_2 data at 10 dbar resolution. Vertically integrated quantities (such as dynamic height) were evaluated with the 2 db resolution data and appended to the analysis data set. The focus of the present work is on the upper 1000 db of the water column, consistent with the NODC data analysis. Contour sections of temperature, salinity and dissolved

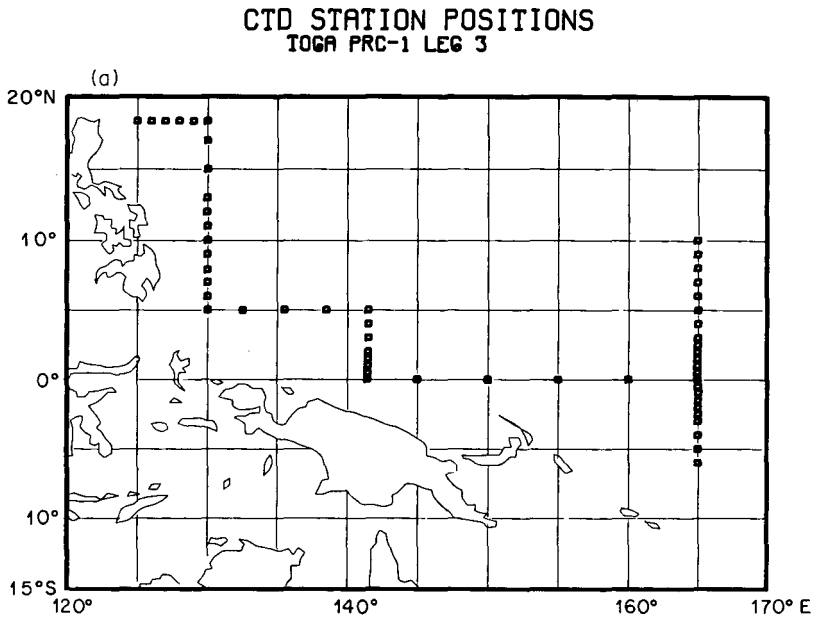

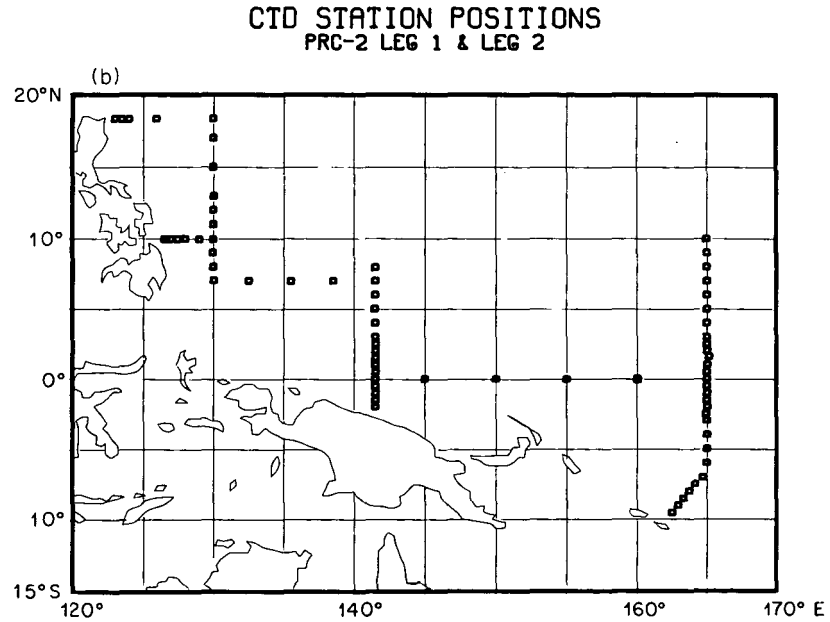

Fig. A1. Section maps for the CTD/O_2 observations obtained during the first two cruises of the US/PRC cooperative program. (a) The first cruise observations: 30 January to 18 February 1987. (b) The second cruise observations: 18 November to 16 December 1987.

oxygen were constructed for the major sections obtained on each cruise. Geostrophic velocity was estimated relative to 1000 db and also mapped. Simple finite differences of dynamic height were taken poleward of 3° latitude. Equatorward of 3°, where station resolution was 1/2°, a binomial filter in the horizontal was applied prior to estimating dynamic height gradients. Velocity at the equator was estimated from the dynamic height curvature at the equator using the smoothed data between 1°N and 1°S (HAYES, 1982). Volume transports were estimated by integrating the velocity data in space as was done for the historical data.